INSTITUTE OF NATURAL AND APPLIED SCIENCES
UNIVERSITY OF ÇUKUROVA

MASTER THESIS

İpek KILIÇCI

UPD (UNDER-POTENTIAL DEPOSITION) AT STEPPED PLATINUM SINGLE CRYSTAL SURFACES

DEPARTMENT OF CHEMISTRY

ADANA, 2009

INSTITUTE OF NATURAL AND APPLIED SCIENCES
UNIVERSITY OF ÇUKUROVA

UPD (UNDER-POTENTIAL DEPOSITION) AT STEPPED PLATINUM SINGLE CRYSTAL SURFACES

By İpek KILIÇCI

A THESIS OF MASTER of CHEMISTRY DEPARTMENT

We cerfity that the thesis titled above was reviewed and approved for the award of degree of the master of physicochemistry by the board of jury on ……

Signature	Signature	Signature .....
Prof.Dr.Birgül Yazıcı	Assoc.Prof.Dr.Gülfeza Kardaş	Assist.Prof.Dr.Muzaffer Özcan
Supervisor	Jury	Jury

This Master Thesis is performed in Chemistry Department of the Instute of Natural and Applied Science of ÇUKUROVA University

Registration Number:

Prof.Dr.İlhami YEĞİNGİL
Director
The Istitute of Natural and Applied Science
Signature and Seal

Not: The usage of the presented specific declarations, tables, figures and photographs either in the thesis or any other reference without citation is subject to'the Law of Intellectual and Arts Products' numbered 5846 of Turkish Republic.

ABSTRACT

MS THESIS

UPD (UNDER-POTENTIAL DEPOSITION) AT STEPPED PLATINUM SINGLE CRYSTAL SURFACES

İpek KILIÇCI

DEPARTMENT OF CHEMISTRY

INSTITUTE OF NATURAL AND APPLIED SCIENCES

UNIVERSITY OF ÇUKUROVA

Supervisor: Prof. Dr. Birgül YAZICI

Year: 2009, **Pages:** 76

Jury: Prof.Dr. Birgül YAZICI

Assoc.Prof.Dr. Gülfeza KARDAŞ

Assist.Prof.Dr. Muzaffer ÖZCAN

It is investigated the underpotential deposition (UPD) of Tl and Pb on stepped Pt single-crystals vicinal to the (100)-surfaces, (like Pt (19,1,1), Pt (11,1,1), Pt (511), Pt (100) and Pt (111)) and the influence of Ru on the CO oxidation on Pt (19,1,1). For Ru deposition two peaks appeared at high potential in the CV in CO free solution. CO oxidation are performed on the Ru free and the Ru modified Pt-surface and it is shown that all peaks shifted to low potential with Ru deposited on the Pt (19,1,1) surface. Instead of one peak for the CO oxidation at 0.75 V on the Ru free Pt (19,1,1), on the Ru modified Pt surface two peaks are visible for the CO adsorbate at 0.58 and 0.63 V. When the potential is stoped at 0.54 V for 3 min., the second peak at 0.7 V is not affected. Tl/Pt (111) the sharpest peak at 0.76 V is explained as a phase-Transition from a $\sqrt{3}x\sqrt{7}$ - to a $\sqrt{3}x\sqrt{3}R30°$ -overstructure of the Tl-Adlayer. Comparison of Tl and Pb has been done and it shows that Tl preferential decorated on step-sites and Pb preferential decorated on terrace-sites. And it is shown that Pb adsorption is more stable at (100) surface than (111) surface.

Keywords : Platinum electrode, Platinum single crystal, CO oxidation, Ru.

ÖZ

YÜKSEK LİSANS TEZİ

BASAMAKLI PLATİN TEK KRİSTAL YÜZEYİNDE DAHA DÜŞÜK POTANSİYELDE BİRİKME

İpek KILIÇCI

ÇUKUROVA ÜNİVERSİTESİ
FEN BİLİMLERİ ENSTİTÜSÜ
KİMYA ANABİLİM DALI

Danışman: Prof. Dr. Birgül YAZICI

Yılı: 2009, **Sayfa:** 76

Jüri: Prof.Dr. Birgül YAZICI

Doç.Dr. Gülfeza KARDAŞ

Yrd.Doç.Dr. Muzaffer ÖZCAN

Bu çalışmada; (100) basamak yüzeyinde (Pt(19,1,1), Pt(11,1,1) ve Pt(511) gibi) Pt tek kristalinin Tl ve Pb UPD'sini ve Pt(19,1,1) yüzeyinde Ru'un CO oksidasyonu üzerinde etkisini araştırdık.Serbest CO çözeltisinde Ru birikimi sırasında siklik voltamogramda (CV) yüksek potansiyelde 2 pik gözlenmiştir. CO oksidasyonu ; Ru içermeyen çözeltide ve Ru içeren çözeltide çalışılmıştır.Bu kıyaslamanın sonucu olarak Ru etkisiyle Pt(19,1,1) yüzeyinde bütün piklerin daha düşük potansiyele doğru kaydığı gözlenmiştir. Pt(19,1,1) yüzeyindeki Ru içermeyen çözeltide CO oksidasyonu sırasında 0.75 V'ta görülen tek pik yerine ; Ru içeren çözeltide 0.58 ve 0.63 V'ta CO adsorpsiyonu gözlenmiştir. Ru içeren çözelti deneyinde; 0.54 V'ta 3 dakikalığına potansiyel akımını durdurduğumuzda 0.7 V'taki 2. pikin etkilenmediği gözlenmektedir.Tl/Pt(111) yüzeyindeki 0.76 V'taki keskin pik $\sqrt{3}x\sqrt{7}$ yapısından $\sqrt{3}x\sqrt{3}R30°$ yapısına faz değiştirdiğini göstermektedir.Tl ve Pb arasında kıyaslama yapılmıştır ve sonuçlar Tl'un özellikle basamağı, Pb'nin ise özellikle terası modife ettiği saptanmıştır. Ayrıca Pb adsorpsiyonunda (100) yüzeyinin (111) yüzeyine göre daha kararlı olduğu saptanmıştır.

Anahtar Kelimeler: Platin elektrodu, Platin tek kristali, CO oksidasyonu, Ru.

ACKNOWLEDGEMENTS

This work was supported by ERASMUS (Student exchange programm).

The authors would like to thank her thesis supervisor Prof.Dr. Birgül YAZICI for having accepted me as s a master student in her group and helped me to go and study at Bonn University.And I want to thank all of members in our Physicochemistry department.

All of the my work performed in electrochemistry department of Bonn University. I went this university for all of my work via Erasmus program. I want to thank a lot Assoc.Prof. Gülfeza Kardaş and our international office for their interest about Erasmus program.

Thanks to all the members of the jury for reading and evaluating my thesis as well as assisting in my exam.

Special thanks to Prof.Dr. Helmut Baltruschat for accepting me for one year in his research group in Bonn.I was very pleased from meet in the airport to end of all my study.When I went there, I met wonderful people there.I never forget their helps.Thank you very much all of Prof.Dr. H. Baltruschat's group for your hospitality.

The author also would like to thank Nicky Bogolowski for his interest about my study and for discussions and corrections.Thank you very much for everything Nicky Bogolowski and all of my group; You are very good friend and very good colleagues.

Finally I would like to thank my family specially my mother for favor and support.

CONTENTS **PAGE**

ABSTRACT……..…... I
ÖZ.....……..... II
ACKNOWLEDGEMENTS…….....…..... III
CONTENTS..... ……..…….…….....IV
TABLE CAPTIONS…….....…….....VII
FIGURES CAPTIONS……..…….....VIII
SYMBOLS AND ABBREVIATIONS……..... XII
1.INTRODUCTION……..... 1
2. THEORETICAL..... 2
2.1. Crystallography of Metals.…….....…….....2
2.1.1. Single Crystal Surfaces..... 4
2.1.2. Miller Indices...……..... 4
2.1.3. Low-Miller-Index Planes of Crystals..... 6
2.1.4. High-Miller-Index Stepped Surfaces...…..... 12
2.2. Surface Structures..... 15
2.2.1. Woods Notation.……..... 15
2.2.2. Relaxation..... 16
2.2.3. Reconstruction..... 17
2.3. Electrochemical Characterization of Single Crystal Surface..... 20
2.4. Cyclic Voltammetry..... 20
2.5. CV Measurements.....…….. 22
2.6. Under-potential Deposition (UPD)..... 23
2.7. Electrode Immersion Technique..... 24
2.8. CO Oxidation..... 24
2.9. Aim of This Work..... 25
2.9.1. Why Thallium and Lead ?..... 25
2.9.1.1. Thallium..... 25
2.9.1.2. Lead..... 26
2.9.2. Why Ruthenium ?..... 27

2.9.2.1. Ruthenium..... 28
3. LITERATURE SURVEY..... 29
3.1. Adsorption Test..... 29
3.2. Hydrogen adsorption on the Low-Indexed Pt ingle-crytals and on stepped single-crystal vicinal to the (100) surface in sulphuric and perchloric acid..... 30
3.3. Tl and Pb UPD..... 34
3.4. Effect of Ru deposition on the CO oxidation at Pt single-crystals..... 37
4. MATERIALS AND METHODS..... 39
4.1. Materials..... 39
4.1.1. Chemicals..... 39
4.1.2. Apparatus..... 40
4.1.3. The Bead Single Crystal Teflon-Holder..... 40
4.1.4. Electrochemical Instrumentation..... 41
4.1.4.1. The Electrodes..... 41
4.1.4.2. The Cell..... 44
4.1.4.3. The Potentiostat..... 44
4.1.5. Glassware..... 45
4.2. Methods..... 46
4.2.1. Preparation of well-ordered noble metal single crystal surfaces..... 46
4.2.2. Calculation of Charge in Cyclic Voltammetry..... 46
5. EXPERIMENTAL RESULTS AND DISCUSSON..... 47
5.1. Tl-UPD on Pt(111), Pt(100), Pt(11,1,1) and Pt(511)..... 47
5.1.1. Voltammetry of the unmodified Pt bead ingle-crystal surfaces in H_2SO_4 solution..... 47
5.1.2. Diffusion controlled Tl-UPD on Pt(111), Pt(100), Pt(511) and Pt(11,1,1)..... 50
5.2. Pb-UPD on Pt(100) and stepped-crystal Pt(19,1,1), Pt(11,1,1) and Pt(511)..... 55
5.2.1. Voltammetry of the unmodified Pt bead single-crystal in $HClO_4$ solution..... 55
5.2.2. Pb-UPD on Pt(100), Pt(19,1,1), Pt(11,1,1) and Pt(511) from $Pb(ClO_4)_2$ containing solution..... 58
5.2.3. Cyclic Voltammetry of Pb/Pt-surfaces in $HClO_4$ solution..... 61
5.3. Effect of Ru submonolayers on the CO oxidation on Pt(19,1,1)..... 62

5.3.1. CO oxidation at the Ru free Pt(19,1,1) surfaces..... 62
5.3.2. Adsorption of Ru submonolayers on Pt(19,1,1) surfaces..... 65
5.3.3. Voltammogram of the Ru/Pt(19,1,1) electrode in H_2SO_4..... 66
5.4. Discussion.....70
6. SUMMARY..... 72
REFERENCES..... 73
CURRICULUM VITAE..... 76

TABLE CAPTIONS **PAGE**

Table 2.1. In the table for stepped surface in the cubic system, stepped-surface designation, Miller indices and 'angle of curt from terrace along zone line toward step' are related……..... 13

Table 4.1. The chemicals that used in this work..... 39

Table 5.1. Charge of various Pt-single crystals for the integration limit is between 0.1 V and 0.45 V..... 49

Table 5.2. Charge of various Pt-ingle crystals..... 57

Table 5.3. Charge density of various Pt-single crystals..... 60

Table 5.4. Charge of various Pt-single crystals.The integration limit is between 0.1 V and 0.5 V..... 62

FIGURE CAPTIONS **PAGE**

Figure 2.1. Five two-dimensional Bravais lattices.Translation vectors a and b are shown..... 2
Figure 2.2. Shows a step, island, terrace, vacancy and adatom..... 3
Figure 2.3. Shows Miller indices calculation..... 6
Figure 2.4. FCC metallic elements structures are shown in yellow at room temperature..... 7
Figure 2.5. Main low-index planes of three basal plane of FCC..... 8
Figure 2.6. Main low-index planes of a FCC..... 8
Figure 2.7. BCC metallic elements structures are shown in yellow at room temperature..... 9
Figure 2.8. Main Low-Index planes of a BCC (body-centred cubic) crystal..... 10
Figure 2.9. Main Low-Index planes of a HCP (hexagonal close-packed) crystal. For the (1010) and (1011) planes, two possible types of surface termination are shown.....11
Figure 2.10. Main Low-Index planes of a diamond crystal..... 11
Figure 2.11. Shows the High-Miller-Index stepped surfaces..... 12
Figure 2.12. a) Stepped (755) and b) Kinked (10,8,7) FCC crystal faces..... 13
Figure 2.13. The stereographic triangle for the FCC system, depicting some of the platinum high index planes present between the low index planes. The arc between (111) and (100) plane is called the [011] zone. On the connection lines the stepped surfaces can be found..... 14
Figure 2.14. Wood's and matrix notation for some super lattices on a hexagonal 2D lattice..... 15
Figure 2.15 Wood's and matrix notation for some super lattices on a square 2D lattice..... 15
Figure 2.16. a) Normal and b) Lateral relaxation in the top atomic layers of a semi-infinite crystal..... 17
Figure 2.17. a) and c) represent the conservative reconstruction. When the number density of surface atom is preserved b) and d) represent the non-

conservative reconstruction in this case when the number density of surface atoms are modified..... 18
Figure 2.18. Hexagonal packing of the top-layer Pt atoms on the square Pt(100) atomic plane..... 19
Figure 2.19. a) An ideal non-reconstructed Pt(110) 1x1 b) Recontructed Pt(110) 2x1 with a missing-row structure..... 19
Figure 2.20. Shows typical voltammogram of the Pt-crystals..... 21
Figure 2.21. The CVs of Pt stepped single crystals Pt(S)[n(100)x(111)] with n=2, 3 and 4 with v=50 mV/s..... 22
Figure 3.1. Scheme of adsorption test..... 29
Figure 3.2. Voltammetric profiles of the Low-indexed Pt(100), Pt(110) and Pt(111) single-crystal surfaces in 0.1 M H_2SO_4 v=50 mV/s..... 31
Figure 3.3. Voltammetric profiles of the Low-indexed Pt(100) and Pt(S)[n(100)x(111)] with n=2, 4 and 6 in 0.1 M H_2SO_4 v=50mV/s..... 32
Figure 3.4. Voltammetric profiles of the Pt(S)[n(100)x(111)] electrodes, with n=3, 4, 8 and 20 and Pt(100) in 0.1 M $HClO_4$ v=50 mV/s. Arrows indicate the increase of the step density..... 33
Figure 3.5. Cyclic voltammograms of the basal planes Pt(111) and Pt(100) in 0.1 M $HClO_4$, v=50 mV/s..... 34
Figure 3.6. Voltammogram of a Pt(111) orientated electrode in contact with an acidic solution of thallium, 5x10-3 M Tl^+ in 0.5 M H_2SO_4 ; sweep rate 20 mV/s..... 35
Figure 3.7. a) Cyclic voltammogram for Pb-UPD in 0.1 M $HClO_4$ on the Pt(100) disk electrode in a RRDE assembly. Base voltammogram without Pb^{+2} in solution under otherwise identical conditions are shown for comparison. b) Ring electrode current with the ring being potentiostated at 0.65 V. Insert integrated charges for the stripping of Pb from the disk electrode assessed from ring (ISC) and disk (TDC) uppdotentiodynamic curves. Rotation rate 900 rpm; sweep rate 50 mV/s..... 36
Figure 3.8. a) Cyclic voltammograms of Pt(111) mounted in the disk position of the RRDE in 0.1 M $HClO_4$ and $5x10^{-5}$ M Pb^{+2} ; rotation rate 900 mV/s,

Sweep rate 50 mV/s b) Ring electrode currents recorded with the ring being potentiostated at -0.59 V..... 37

Figure 3.9. Shows the CV of oxidation of adsorbed CO at Pt(111) covered by (submonolayers of) Ru and Sn. CVs are shown in 3.9.a ; MSCVs (massspectrometry cyclic voltammetry) for CO_2 are shown in 3.9.b dE/dt=10 mV/s, 0.5 M H_2SO_4 (__) deposition of Ru followed by deposition of Sn (- - -) deposition of Sn followed by deposition of Ru (-,-,-) only deposition of Sn (. . .) bare Pt-surface for comparison... 38

Figure 4.1. The Pt-electrodes with Teflon-holder..... 41

Figure 4.2. Potentiostat/Galvonostat Model 273..... 45

Figure 5.1. Recorded CVs of the two basal plane single-crystals in 0.1 M H_2SO_4 with v=50mV/s..... 48

Figure 5.2. CVs of Pt stepped single crystals Pt(S)[n(100)x(111)] with n=3, 6 and Pt(100) in 0.1 M H_2SO_4..... 49

Figure 5.3. The CVs for Tl/Pt(111) in 10^{-3} M Tl_2SO_4+0.1 M H_2SO_4 with v=10 mV/s..... 51

Figure 5.4. The CVs for Tl deposition (__) on Pt(11,1,1) in 10^{-6} M Tl_2SO_4+0.1 M H_2SO_4 and after preparation (. . .) with v=50 mV/s..... 52

Figure 5.5. The CVs for Tl deposition (__) on Pt(511) in 10^{-6} M Tl_2SO_4+0.1 M H_2SO_4 and (. . .) after preparation in 0.1 M H_2SO_4 with v=50mV/s..... 53

Figure 5.6. The CVs for Tl deposition (__) on Pt(100) in 10^{-6} M Tl_2SO_4+0.1 M H_2SO_4 and (. . .) after preparation in 0.1 M H_2SO_4 with v=50mV/s..... 54

Figure 5.7. The CVs for Tl deposition (__) on Pt(111) in 10^{-6} M Tl_2SO_4+0.1 M H_2SO_4 and (. . .) after preparation in 0.1 M H_2SO_4 with v=50mV/s.... 55

Figure 5.8. Voltammetric profiles of the Pt(S)[n(100)x(111)] electrodes, with n=3,6 and 10 and Pt(100) in 0.1 M $HClO_4$. v= 50 mV/s..... 56

Figure 5.9. Recorded CVs Pt(111) in 0.1 M $HClO_4$. v= 50 mV/s..... 57

Figure 5.10. Voltammetric profiles of the Pt(S)[n(100)x(111)] electrodes, with n=3,6 and 10 and Pt(100) in 10-3 M $Pb(ClO_4)_2$+0.1 M $HClO_4$ a) v= 50 mV/s b) v=10 mV/s..... 59

Figure 5.11. CVs for Pt(111) in 10^{-3} M $Pb(ClO_4)_2$+0.1 M $HClO_4$ with a) v=50 mV/s b) v= 10 mV/s..... 60
Figure 5.12. Voltammetric profiles of the Pt(S)[n(100)x(111)] electrodes, with n=3,6 and 10 and Pt(100) after Pb-UPD in 0.1 M $HClO_4$ with v= 50 mV/s.....61
Figure 5.13. CVs for Pt(111) after Pb-UPD in 0.1 M $HClO_4$ with v=50 mV/s..... 62
Figure 5.14 Recorded CVs for after preparation of Pt(19,1,1) in 0.1 M H_2SO_4 v=50 mV/s..... 63
Figure 5.15. The first CV for Pt(19,1,1) after CO oxidation in 0.1 M H_2SO_4 with v= 10 mV/s..... 64
Figure 5.16. CV for the Pt(19,1,1) for after CO oxidation in 0.1 M H_2SO_4 with v=50 mV/s..... 65
Figure 5.17. CVs for Ru deposition at Pt(19,1,1) in 10^{-5} M $RuCl_3$+0.1 M H_2SO_4 with v= 50 mV/s..... 66
Figure 5.18. The CVs for Ru/Pt(19,1,1) in 0.1 M H_2SO_4..... 67
Figure 5.19. The CVs for CO oxidation in 0.1 M H_2SO_4 with v=10mV/s..... 68
Figure 5.20. The CV for CO oxidation of Pt(19,1,1) with v=10mV/s..... 69
Figure 5.21. The CV for the Pt(19,1,1) (. . .) after CO oxidation and (__) after Ru/Pt in 0.1 M H_2SO_4 with v=50 mV/s..... 69
Figure 5.22. Compares the CO oxidation (. . .) Ru free surface and (__) Ru containing solution with v=10 mV/s..... 70

SYMBOLS AND ABBREVIATIONS

V : Volt

E : Electrod potential (V)

F : Faraday constant (96485 $C.mol^{-1}$)

I : Ionic current (mA/cm^2)

η : Over voltage (V)

μC : Micro Coulomb

P_o : Nernst potential

P_{oo} : Standard potential

Z : Number of transferred electrons

Pt : Platinum

Tl : Thallium

Pb : Lead

Ru : Ruthenium

UPD : Under-potential deposition

Q_F : Faradic charge

FCC : Face-centred cubic

BCC : Body-centred cubic

HCP : Hexagonal close-packed

1. INTRODUCTION

The adsorption of adatoms on metal electrodes and underpotential deposition has been studied in electrochemical research. It is wanted studied with Tl and Pb to observe their behaviour on Pt surfaces. It is wanted obtain that these metals can decorate on step sites or terrace sites. Subsequent Pt single-crystals are prepared by heating and cooling in pure water saturated by hydrogen .It can be modified with these metals under-potential control adsorption from a metal containing solution.

In combination with Pt, ruthenium has good catalytic properties for the CO in fuel cells. Ruthenium is often studied on Pt single-crystal surface with defined surface geometry because of this it is wanted study Pt(S)[n(100)x(111)] n= 10 electrodes. After heating and cooling down in a hydrogen atmosphere over MilliQ-water process it can be modified with Ru under potential control adsorption from a ruthenium containing solution.

Adsorption is the collection of atoms or molecules on the surface of a material. It creates a film of the adsorbate on the adsorbent`s surface. Adsorption/desorption process are main amount of the solid/gas or solid/liquid interfaces.

There are two important differences between metal-gas and metal-solution interfaces.

The first one is that the gas which is a dilute phase is replaced by solution which is a concentrated phase; for electrolytic systems, adsorption always corresponds to a replacement process.

The second one is the greater convenience by which the local field may be varied at the electrochemical interface than at the gas-solid interface.

2. THEORETICAL

2.1. Crystallography of metals

Crystals consist of periodic repetitions of identical cells each containing one or more atoms. The unit cell which can be used for construct the crystal is the smallest cell.

2-dimensional crystal with a rectangular unit cell containing a single atom.

Bravais Lattice

The same lattice as above generated from a different choice of unit cell.

If the unit cell contains a single atom, the cell is called *primitive* and the lattice is a *Bravais lattice*.Following the figure 2.1. is related to Bravais lattices.

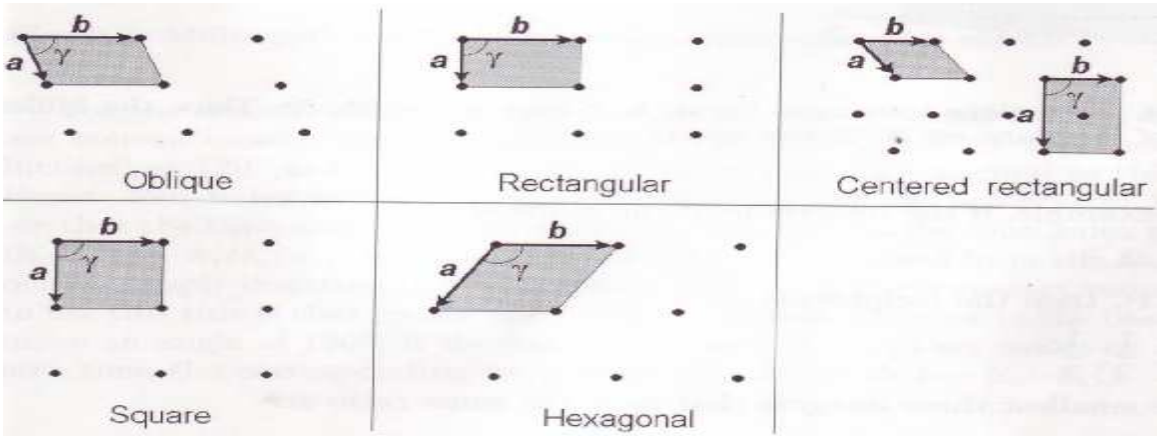


Figure 2.1. Five two-dimensional Bravais lattices. Translation vectors a and b are shown.

Lattice planes

A lattice contains a large number of planes of atoms. These planes are named using the Miller indices (n_i , n_j , n_k) defined with the convention that the vector.

$$\mathbf{r} = n_i\mathbf{i} + n_j\mathbf{j} + n_k\mathbf{k}$$

is a normal vector for the plane. In this equation **i**, **j** and **k** are the basis vectors and n_i, n_j, and n_k are integers. This is 3D *(three-dimensional)* Lattices plane**.**

Real surfaces, as opposed to the ideal surfaces described below, one characterized by steps and terraces. The steps can be one or many rows of atoms. The step also need not be straight, that gives rise to kinks. Single atoms or adatoms may stay anywhere on a terrace. There can be also vacancies in the terrace, leaving small holes in the surface. These holes are indicated by the dotted cubes [G.A. Somorjai,(1994)] [T. Michely and G. Comsa,(1991)].

This is a simple model of a real surface and typical STM images are shown. As indicated below, a main cause for the existence of steps on a single crystal surface is a (small) misorientation as a result of cutting and polishing. Sometimes such a miscut is formed willfully, in order to obtain surfaces with nearly equidistant monoatomic high steps and terraces of a certain average width [G.A. Somorjai,(1994)].

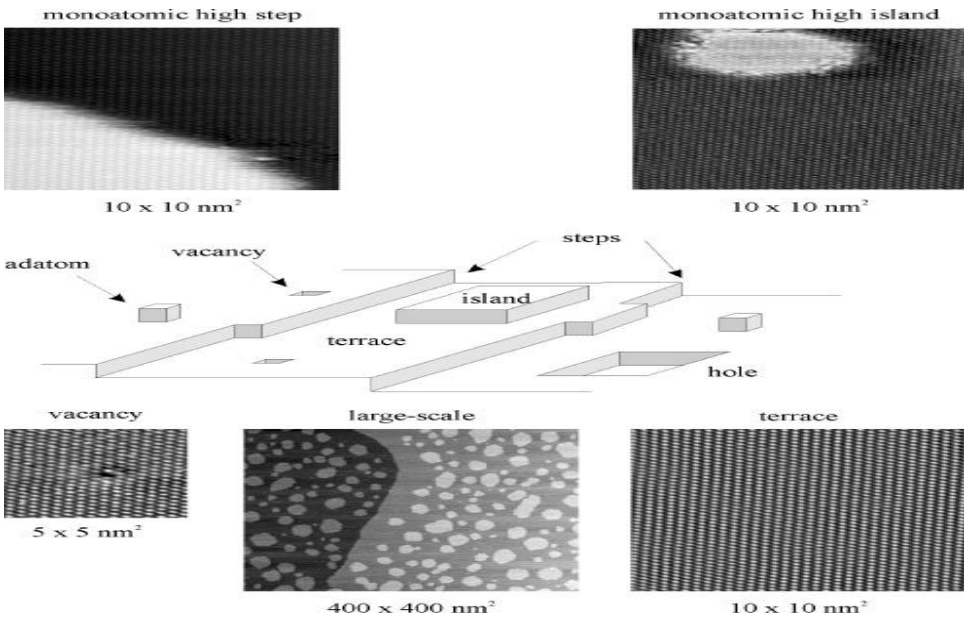


Figure 2.2. *S*hows a step, island, terrace, vacancy and adatom [L. A. Kibler, (2003)].

2.1.1. Single Crystals Surface

Due to the known regular surface geometry, Pt single crystal electrodes are suited model systems for the analysis of the relationship between the surface structure and the surface reactivity.

The crystal itself is composed of regularly repeating structural motives (e.g., atoms, molecules). In the ideal case, the space lattice three-dimensional infinite array of atoms is surrounded in an identical way by its neighbours with a periodicity free from defects. The crystal structure itself is obtained by associating with each lattice point into an identical structural motive.

2.1.2. Miller Indices

Miller indices were introduced in 1839 by the British mineralogist William Hallowes Miller. The method was also historically known as the Millerian system.

The certain meaning of this notation depends upon a choice of lattice vectors for the crystal, as described below. Usually, three primitive lattice vectors are used. Although, for cubic crystal systems, the cubic lattice vectors are used even when they are not primitive (e.g., as in BCC (body-centred) and FCC (face-centred crystals)).

A system of notation called Miller indices that provides a short , unequivocal numeral label for all rational crystal planes. Rational crystallographic planes are defined by a set of rational lattice points, which in turn are specified by the primitive lattice vectors.

If each atom in the crystal is represented by a point and these points are connected by lines, the resulting lattice may be divided into a number of blocks, or unit cells; the intersecting edges of one of the unit cells defines a set of crystallographic axes, and the Miller indices are determined by the intersection of the plane with these axes. The reciprocals of these intercepts are computed, and fractions are giving the three Miller indices (*hkl*) [N. Tian, (2008)].

Where a surface plane has unequal contributions from two different basal planes of the unit cell cube, a stepped surface is obtained, for example, (100) planes separated by (110) steps. Also , if the surface plane has unequal contributions from all three planes of the unitcell cube a kinked surface is obtained by characterised for example , (100) planes separated by kinks of (110) and (111) symmetry. The ratio of the contributions of the different planes of the unit cell cube when determines sizes of the different domains [A. L. Spek, (2003)].

Now it can be explained the Miller İndices with example. They are:
Determine the intercepts of the face along the crystallographic axes, in terms of unit cell dimensions.

1 Take the reciprocals
2 Clear fractions
3 Reduce to lowest terms

For example, if the x-, y-, and z- intercepts are 2, 1, and 3, the Miller indices are calculated as;

1 Take reciprocals: 1/2, 1/1, 1/3
2 Clear fractions {multiply by 6}: 3, 6, 2
3 Reduce to lowest terms (already there)

Thus, the Miller indices are 3, 6, 2.Following the figure is related to Miller indices calculation.

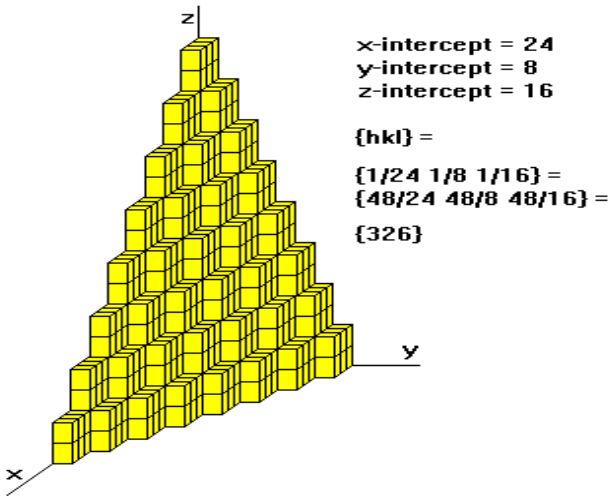


Figure 2.3. Shows Miller indices calculation.

Some General Principles

♦ When the plane is parallel to the axis, its intercept is at infinity the Miller index is '0' (zero).

♦ When the plane is more nearly parallel to the axis, the Miller index is smaller.

♦ When the plane is more nearly perpendicular to the axis, the Miller index is larger.

♦ Multiplying or dividing a Miller index by a constant has no effect on the orientation of the plane.

♦ Miller indices are almost small.

2.1.3. Low-Miller-Index Planes of Crystals

The FCC (Face-centred-cubic) Lattice : Bulk structure

The face centred lattice equals the simple cubic lattice with the addition of a lattice point in the centre of each of the six faces of each cube. This cell contains 4 atoms. It is conventional and cubic, the FCC lattice can be build from a primitive cell. But the primitive cell is inconvenient for many purposes. For example it is a parallelepiped and not cubic. Also, the crystallographic directions are defined with

regard to the conventional cell. **(**FCC) unit cell there is one host atom at each corner and one host atom in each face. Since each corner atom contributes one eighth of its volume to the cell interior, and each face atom contributes one half of its volume to the cell interior (and there are six faces), then $Z = {}^{1}/_{8}\cdot 8 + {}^{1}/_{2}\cdot 6 = 4$.

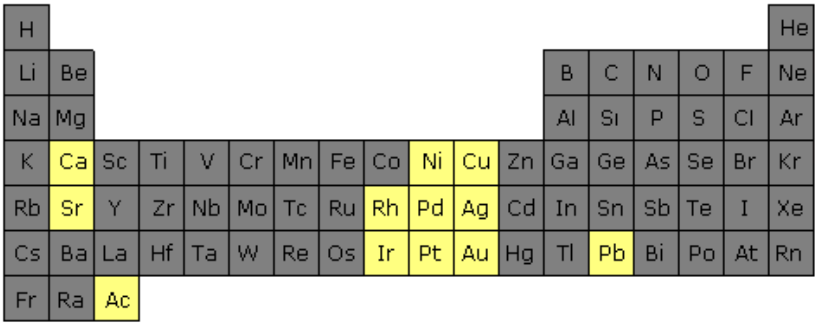


Figure 2.4. FCC metallic elements structures are shown in gray at room Temperature [http://www.mateck.de].

The FCC (100) surface

Atoms in the first layer have 8 neighbours. The (100) surface is that obtained by cutting the FCC metal parallel to the front surface of the FCC cubic unit cell - this exposes a surface (the atoms in blue) with an atomic arrangement of 4-fold symmetry.

The FCC (110) surface

This surface is the most open surface of the three basal planes for FCC.

In the first layer atoms have 7 neighbours. But in the second layer atoms have 11 neighbours [http://www.mateck.de]. The (110) surface is obtained by cutting the FCC unit cell in a manner that intersects the *x* and *y* axes but not the *z*-axis - this exposes a surface with an atomic arrangement of 2-fold symmetry.

The FCC (111) surface

In the first layer atoms have 9 neighbours. The (111) surface is obtained by cutting the FCC metal in such a way that the surface plane intersects the *x*-, *y*- and *z*-axes at the same value - this exposes a surface with an atomic arrangement of 3-fold (apparently 6-fold, hexagonal) symmetry. This layer of surface atoms actually corresponds to one of the close-packed layers on which the FCC structure is based.

The topmost atoms are shown by number 1, the atoms in the deeper layers by number 2 and 3 in the figure 2.5.

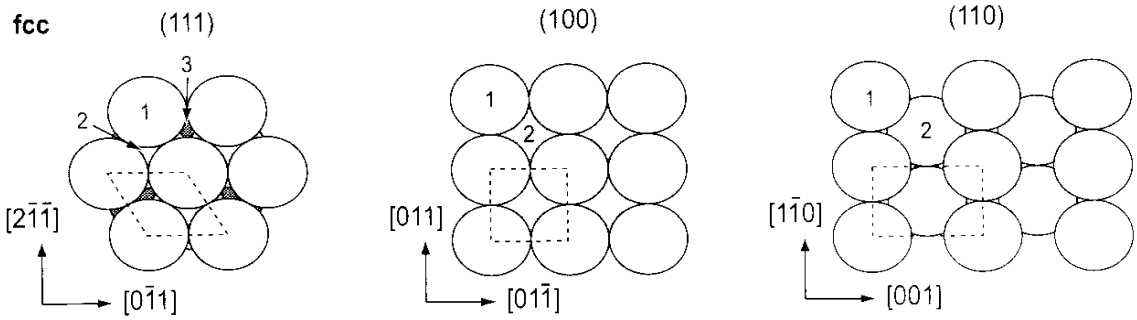


Figure 2.5. Main low-index planes of three basal plane of FCC

In figure 2.6. shows the main low-index planes of a face-centred cubic cell.

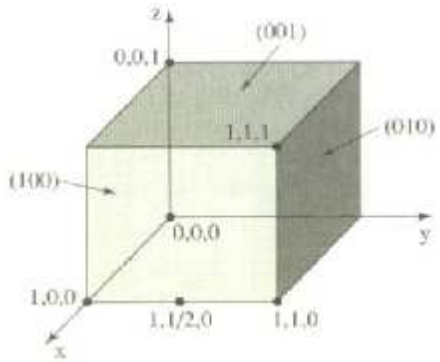


Figure 2.6. Main low-index planes of a FCC

BCC (Body-centred cubic) Lattice : Bulk

The body centred lattice equals the simple cubic lattice with the addition of a lattice point in the centre of each cube. The figure 2.7. shows the conventional unit cell for BCC, this cell is cubic and contains 2 atoms. Each atom has 8 neighbours.

(BCC) unit cell there is one host atom (lattice point) at each corner of the cube and one host atom in the centre of the cube: Z = 2. Each corner atom touches the central atom along the body diagonal of the cube, and it is easy to show by that the unit cell edge, an irrational number, is about 2.3r. Thus, the corner atoms do not touch one another.

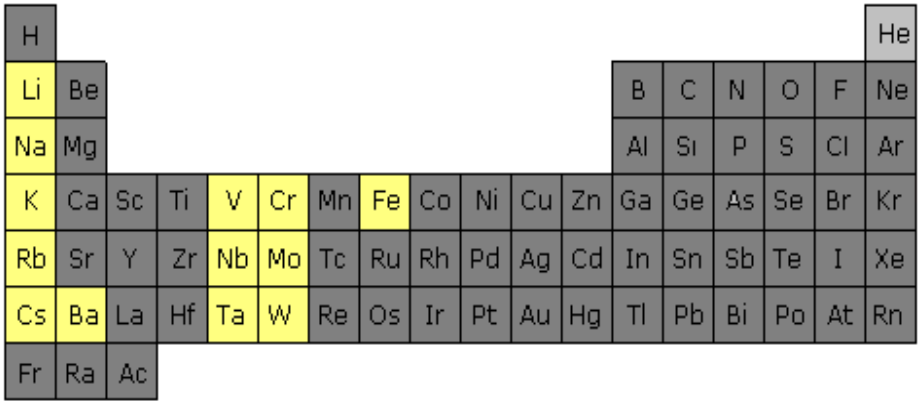


Figure 2.7. BCC metallic elements structures are shown in gray at room temperature [http://www.mateck.de].

The BCC (100) surface

In the surface plane each surface atom has 4 neighbours and 1 neighbour in the plane below the figure 2.8. [http://www.mateck.de].

The BCC (110) surface

In the surface plane each surface atom has 4 neighbours and 2 neighbours in the plane below. This surface plane is the most open of the three planes for BCC.

The BCC (111) surface

In the first layer atoms have 3 atoms in the second layer and 1 neighbour in the third layer. In the second layer atoms have 3 neighbours in the first layer, 3 neighbours in the second layer and 1 neighbour in the third layer. This surface is very open**.**

In the figure 2.8. the atoms in the top layer present a rather "open" arrangement of atoms with poor packing efficiency. This surface often reconstructs. The (110) surface has pseudo-hexagonal packing. Four sides of each hexagon have equal length while the remaining two are longer. The (111) surface has hexagonal packing but is a very rough surface.

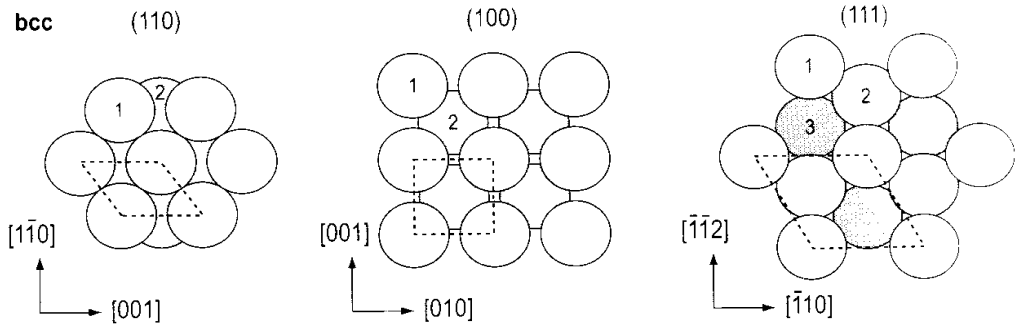


Figure 2.8. Main low-index planes of a BCC (body-centred cubic) crystal [http://www.mateck.de].

HCP (Hexagonal close-packed)

With hexagonal crystal systems, it is possible to use the Bravais-Miller index which has 4 numbers (*h k i l*).

i = -h - k

h , k and l are identical to the Miller index , and i is a redudant index.The HCP (0001) surface is very similar to the FCC (1,1,1) surface.The odd difference occurs deeper into the surface. It can be explained with this example; (110) ≡ (112□0) and (12□0) ≡ (12□10) is more obvious when the redundant index is shown ;

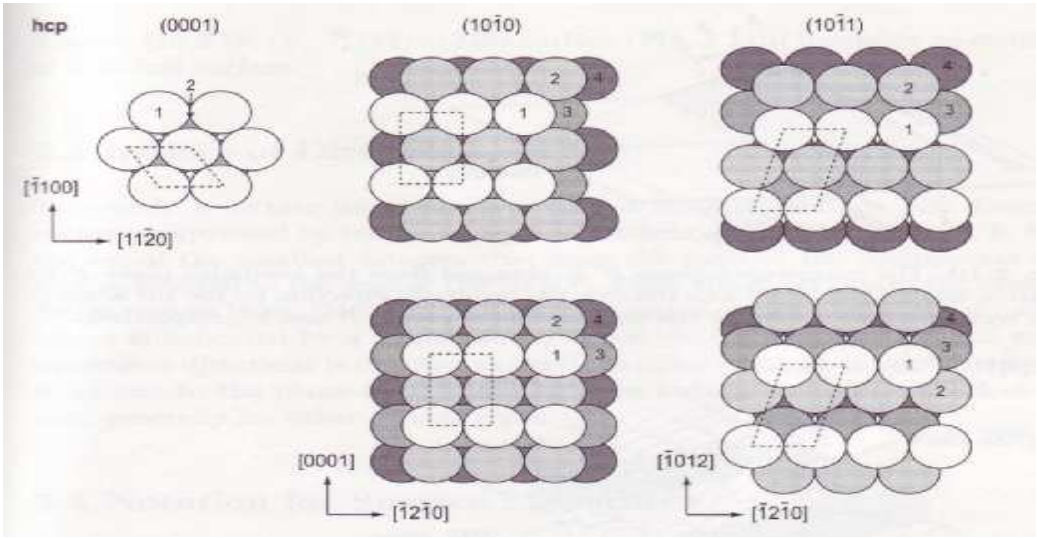


Figure 2.9. Main low-index planes of a HCP (hexagonal close-packed) crystal. For the (1010) and (1011) planes, two possible types of surface termination are shown.

The diamond lattice consists of a face-centred cubic Bravais point lattice which contains two identical atoms per lattice point. The distance between the two atoms equals one quarter of the body diagonal of the cube. The diamond lattice represents the crystal structure of diamond, germanium and silicon.

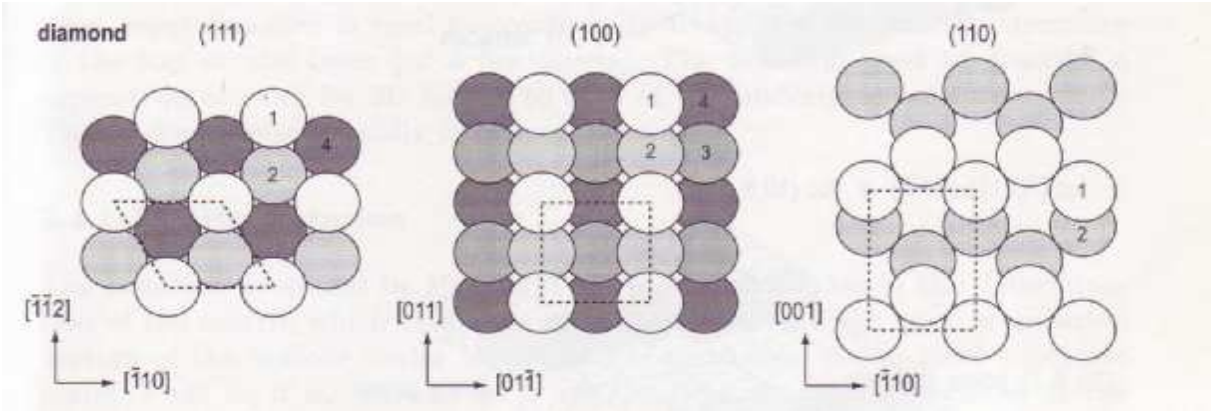


Figure 2.10. Main low-index planes of a diamond crystal.

2.1.4. High-Miller-Index Stepped Surfaces

High Miller index surfaces have been studied less than low Miller index crystal surfaces. The few studies that have been made using metal, semiconductor and oxide surfaces revealed that these surfaces are structurally heterogeneous.The figure 2.11. shows High-Miller-Index Stepped surface.

♦ If the crystal surface is misoriented from the low-index plane by a small angle, it can be described by the combination of three parameters: tilt angle, tilt azimuth and tilt zone.

♦ The tilt zone specifies the axis, around which the rotation from the basal low-index plane to the tilted plane is conducted.

♦ The azimuth specifies the direction of the rotation.

♦ The tilt angle specifies the angle of rotation [G. Somorjai and D. W. Blakely, (1997)].

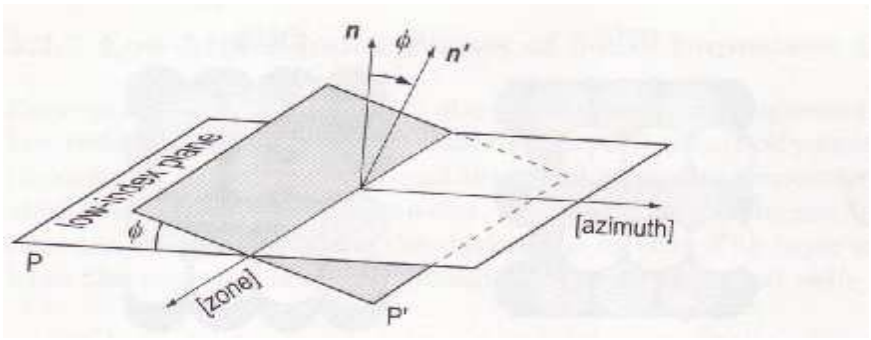
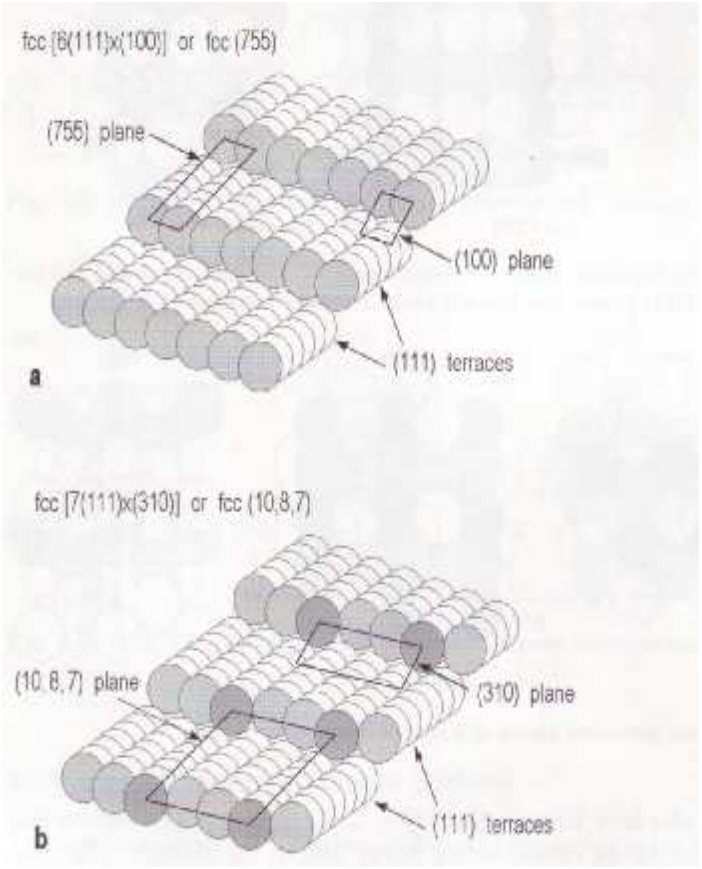


Figure 2.11. Shows the High-Miller-index stepped surfaces

The atomic structures of high-Miller-index surfaces are composed of terraces, separated by steps, which may have kinks in them. Thus, the (755) surface of an FCC crystal consist of (111) terraces, six atoms deep, separated by straight steps of (100) orientation and of single-atom height. The FCC (10,8,7) has kinks in its step edges, the steps are not straight. The steps and kinks provide a degree of roughness that can be very important [D. W. Blakely and G. A. Somorjai, (1977)] [S. T. Pratt, (2005)].



a) Stepped (755)

b) Kinked (10,8,7) Fcc faces

Figure 2.12. a) stepped (755) and **b)** Kinked (10,8,7) FCC Crystal Faces

Table 2.1. The table shows types of stepped surface in cubic system, 'stepped-surface Designation', 'Miller indices' ,and 'angle of curt from terrace along zone line toward step' are related [G. Somorjai and D. W. Blakely, (1977)].

Table 3
Types of Stepped Surfaces in Cubic System

Stepped-surface designation	Miller indices	Angle of cut from terrace along zone line toward step
$n(111)-(111)$ Example: 9(111)–(111)	$(n, n, n-2)$ (997)	$\tan^{-1}\left(\frac{2\sqrt{2}}{3n-2}\right)$ 6.45°
$n(111)-(100)$ Example: 10(111)–(100)	$(n+1, n-1, n-1)$ (11, 9, 9)	$\tan^{-1}\left(\frac{2\sqrt{2}}{3n-1}\right)$ 5.57°
$n(100)-(111)$ Example: 10(100)–(111)	$(2n-1, 1, 1)$ (19, 1, 1)	$\tan^{-1}\left(\frac{\sqrt{2}}{2n-1}\right)$ 4.25°
$n(100)-(110)$ Example: 9(100)–(110)	$(n, 1, 0)$ (910)	$\tan^{-1}\left(\frac{1}{n}\right)$ 6.34°
$n(110)-(111)$ Example: 5(110)–(111)	$(2n-1, 2n-1, 1)$ (991)	$\tan^{-1}\left(\frac{\sqrt{2}}{2(2n-1)}\right)$ 4.49°
$n(110)-(100)$ Example: 9(110)–(100)	$(n, n-1, 0)$ (980)	$\tan^{-1}\left(\frac{1}{2n-1}\right)$ 3.37°

This is the some of the most important angles between the planes.

For example, a Pt (19,1,1) single crystal surface, can also be labelled as a Pt(S)[10(100)x(111)] with 10 atoms wide (100) terraces and a single atom high (111) steps. In the FCC system, all planes can be described by various combinations of the three FCC basal planes (111), (110) and (100). The smooth transition in the voltammograms, on going from one low index plane to another around the stereographic triangle (Fig. 2.13), via intermediate high index planes, is apparent.

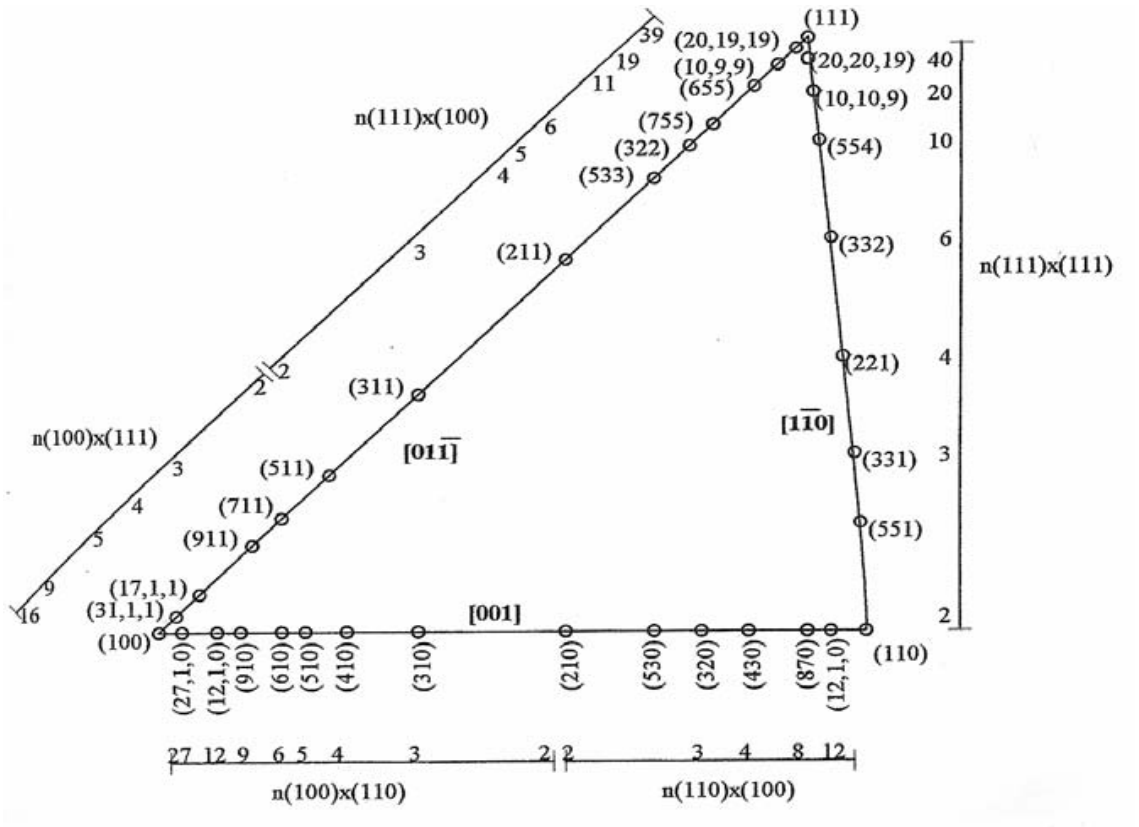


Figure 2.13. The stereographic triangle for the FCC system, depicting some of the platinum high index planes present between the low index planes .The arc between (111) and (100) plane is called the $[0\,1\bar{1}]$ zone. On the connection lines the stepped surfaces can be found [G. Somorjai and D. W. Blakely, (1977)].

2.2. Surface Structures

2.2.1. Wood's Notation

Wood's notation is the simplest and most frequently used method that describes a surface structure. It only works, however, if the two unit cells are the same symmetry or closely-related symmetries. The ratio of lengths of the supper lattice and substrate lattice vectors, and angle of rotation between them. In addition , one indicates the angle of rotation which makes the unit mesh of the surface to be aligned with the basic translation vectors substrate.

Some examples

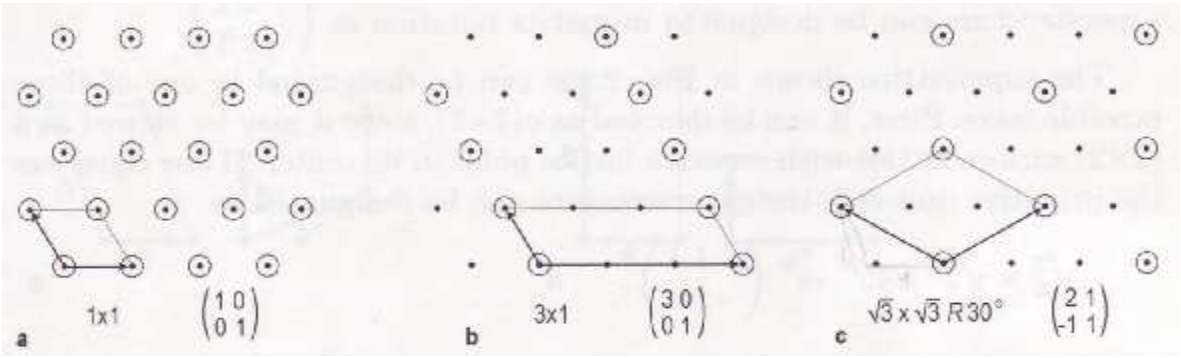


Figure 2.14. Wood´s and matrix notation for some super lattices on a hexagonal 2D lattice.

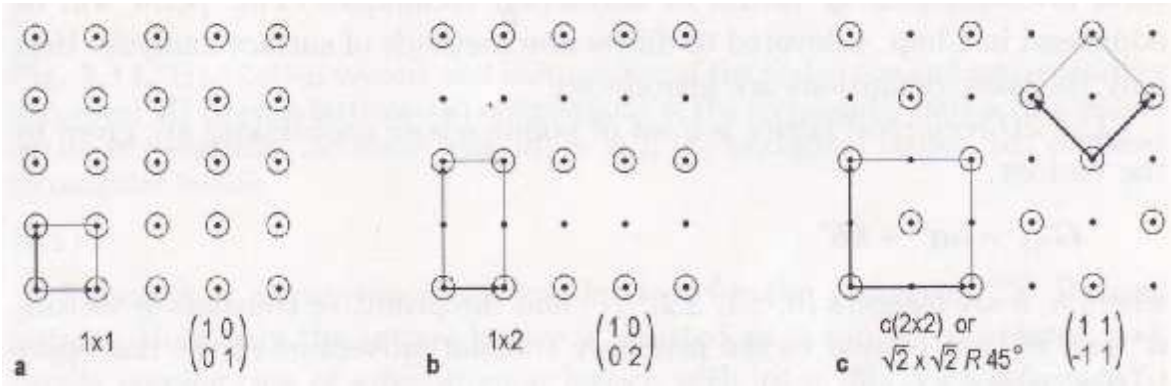


Figure 2.15. Wood´s and matrix notation for some super lattices on a square 2D lattice

Matrix Notation

This is a much more general system of describing surface structures which can be applied to all ordered over layers: quite simply it relates the vectors $\mathbf{b_1}$ & $\mathbf{b_2}$ to the substrate vectors $\mathbf{a_1}$ & $\mathbf{a_2}$ using a simple matrix i.e.

$$\begin{pmatrix} \mathbf{b}_1 \\ \mathbf{b}_2 \end{pmatrix} = \begin{pmatrix} * & * \\ * & * \end{pmatrix} \begin{pmatrix} \mathbf{a}_1 \\ \mathbf{a}_2 \end{pmatrix}$$

$\mathbf{a_1}$, $\mathbf{a_2}$, $\mathbf{b_1}$ and $\mathbf{b_2}$ are vectors.

Dimension of Matrix

The dimensions of a matrix refer to the number of rows and columns of a given matrix. By convention the dimension of a matrix are given by;
number of rows • number of columns
[L. C. Ward and J. L. Stickney, (2001)]

Due to the absence of neighbouring atoms on one side, the forces acting on the surface atoms are modified. Therefore, one expects that the equilibrium structure of the top atomic layer differs from the corresponding atomic plane in the bulk. Two general types of atomic rearrangements are identified as:

1) Relaxation
2) Reconstruction

2.2.2. Relaxation

When the atomic structure of the topmost layer is the same as in the bulk but the first interlayer spacing are modified, is defined as **normal relaxation**. In addition to normal relaxation, sometimes uniform displacement of the topmost layers parallel to the surface takes place. This case is defined as **parallel** or **tangential relaxation** [K. Swammy, (1999)].

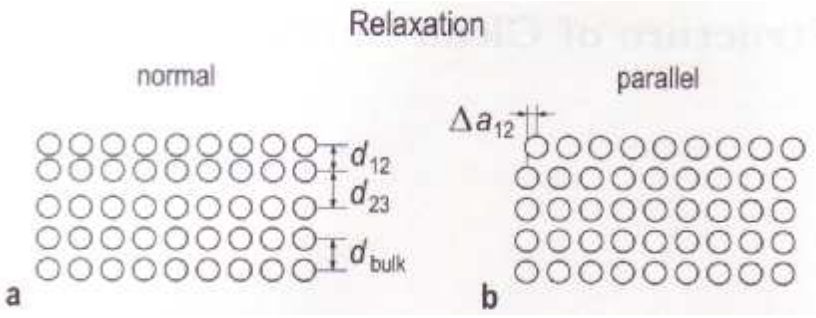


Figure 2.16. a) Normal **b)** lateral relaxation in the top atomi c layers of a semi-infinite crystal

2.2.3. Reconstruction

When the atomic structure of the top layer is modified is referred to as **reconstruction**. It is depending on the number of atoms in the top layer is preserved or not, two types namely ,

1) Conservative reconstructions
2) Non-conservative reconstructions

1) The number of atoms is conserved and reconstruction contains only displacement of surface atoms from the ideal sites.
2) The number of atoms in the reconstructed layer is changed in comparison with the bulk [S. J. Jenkins, (2001)].

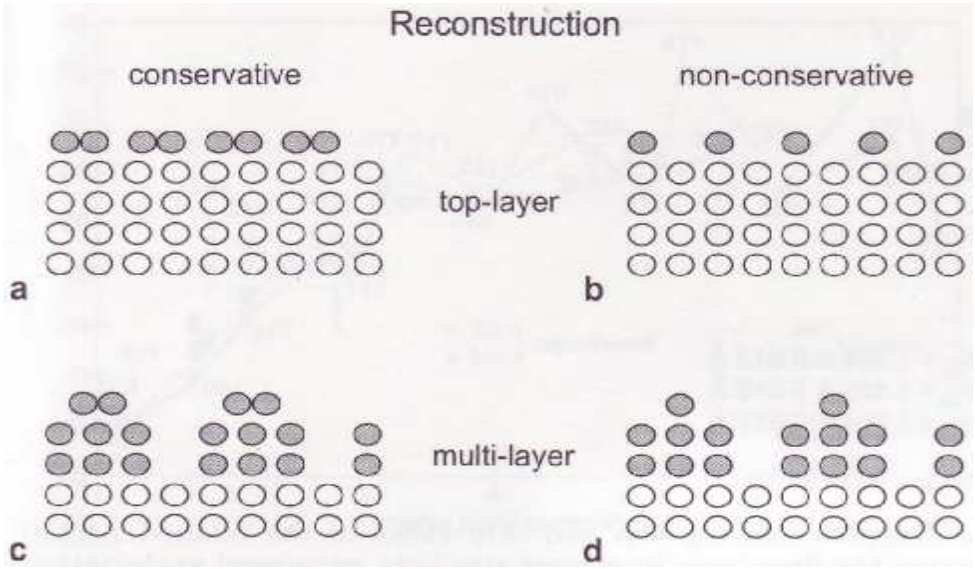


Figure 2.17. **a)** and **c)** represent the conservative reconstruction When the number density of surface atoms is preserved **b)** and **d)** represent the non-conservative reconstruction in this case when the number density of surface atoms are modified.

Reconstructed Surface of Metals

In contrast to most metal surfaces, which are not reconstructed, the surfaces of some noble and near-noble FCC metals, Au, Ir and Pt and BCC transition metals, W and Mo , display reconstructions [V. Fiorentini, (1993)].

Pt (100)

Platinum is a FCC metal and ideal non-reconstructed (100) surface comprises an arrangement of atoms forming a square lattice. An ideal Pt (100) surface is loosely packed and is subjected to a large tensile stress unstable.

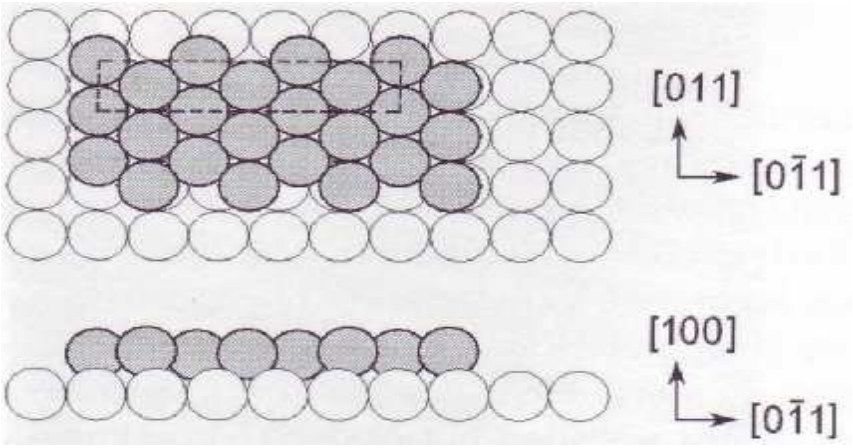


Figure 2.18. Hexagonal packing of top-layer Pt atoms on the square Pt (100) atomic plane.

Pt (110)

An ideal (110)-terminated FCC structure consists of atoms arranged in rows along the (110) direction. Doubled periodicity at Pt (110) is due to the missing-row-structure [S. J. Jenkins, (2001)] [R. Michaelis and D. M. Kolb, (1992)].

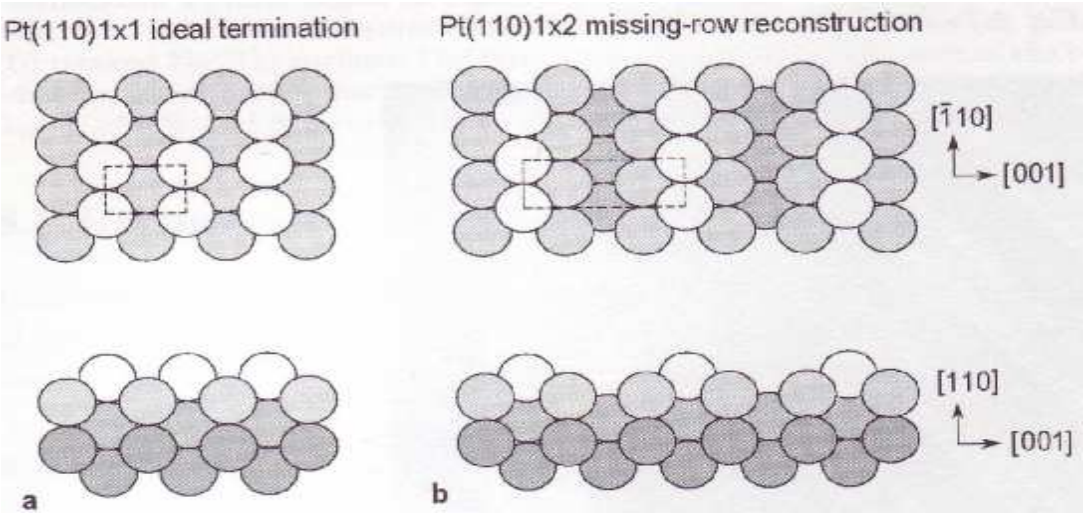


Figure 2.19. a) An ideal non-reconstructed Pt (110)1x1 **b)** reconstructed Pt (110)2x1 with a missing-row structure.

2.3. Electrochemical characterization of single crystal surfaces

First of all working under clean conditions is the most important thing of well-prepared single crystal surfaces. Because of this electrochemical cells must be cleaned. For many electrochemical experiments, the freshly prepared electrode must be immersed into the electrolyte under potential control, for example to preserve the thermally induced reconstruction. The initial potential should chose to lie in the double-layer region. Because in this region there is no Faraday reactions take place. Nevertheless, the electrode surface remains are not always unchanged upon immersion into the electrolyte under potential control and because of this it is an important and it depends on potential and solution composition [K. Sashikata, (1991)], [J. Clavilier, (1980)].

2.4. Cyclic voltammetry

This is the simplest and most commonly used technique.It is a type of potentiodynamic electrochemical measurement and it is ideal for a first characterization of metal/electrolyte interfaces. Current-potential curves can be used as fingerprints and allow to get a general idea of the surface quality. Under examination the electrode potential is cycled between two potential limits at a constant scan rate. Plotting the measured current density versus the electrode potential gives typical voltammograms (CV) e.g. for hydrogen, oxygen and anion adsorption [L. A. Kibler, (2003)].

Different stepped surfaces were subsequently studied by cyclic voltammetry. In particular, through the extensive work of Clavilier et al. the different single crystal platinum surface were investigated and the relationship between hydrogen adsorption-desorption and Pt single crystal surface structure was quantitatively analyzed. The experimental results have shown that the structure sensitive hydrogen adsorption/desorption varies systematically with changing indices and that such voltammograms can be used as a reference for in situ surface characterization. Such

a general survey of voltammograms for various surfaces of platinum single crystals is depicted.

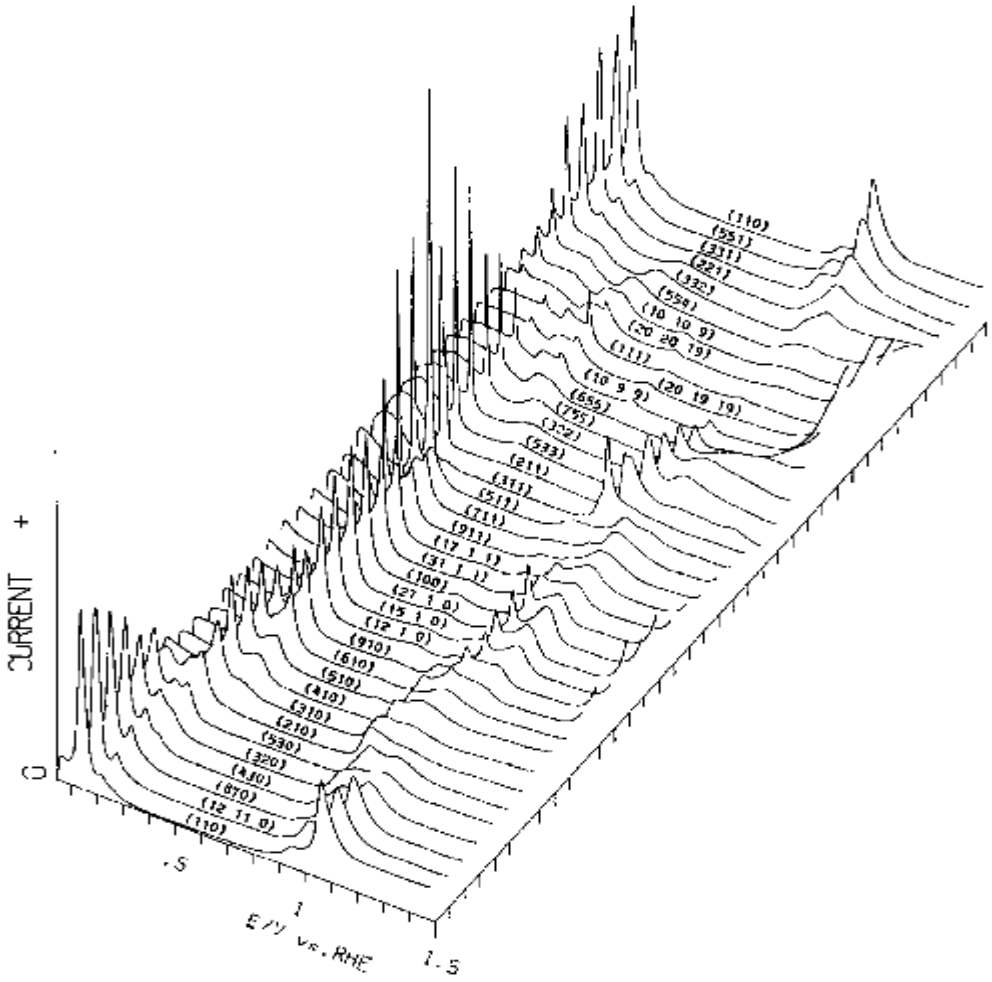


Figure 2.20. Shows typical voltammogram of the Pt-crystals [N. Furuya and S. Koide, (1989)].

Blank voltammograms

The potential ranges were chosen with respect to hydrogen evolution, which starts at 0.06 V, and the beginning oxidation of Pt(100) over 0.8 V, which causes damage to the surface order and therefore should be avoided.

Examples are given in the figure 2.21. where it can be seen that the current profile mainly consists of three contributions. The current from 0.06 to 0.2 V has

been ascribed to hydrogen adsorption/desorption on (111)-steps, from 0.25 to 0.33 V to competitive anion/hydrogen adsorption/desorption on (100)-terrace edges and from 0.33 to 0.43 V to the latter process on (100)-terraces. It is clearly visible that contributions due to processes related with steps increase with the step density, while those related with processes on terraces diminish with the terrace width.

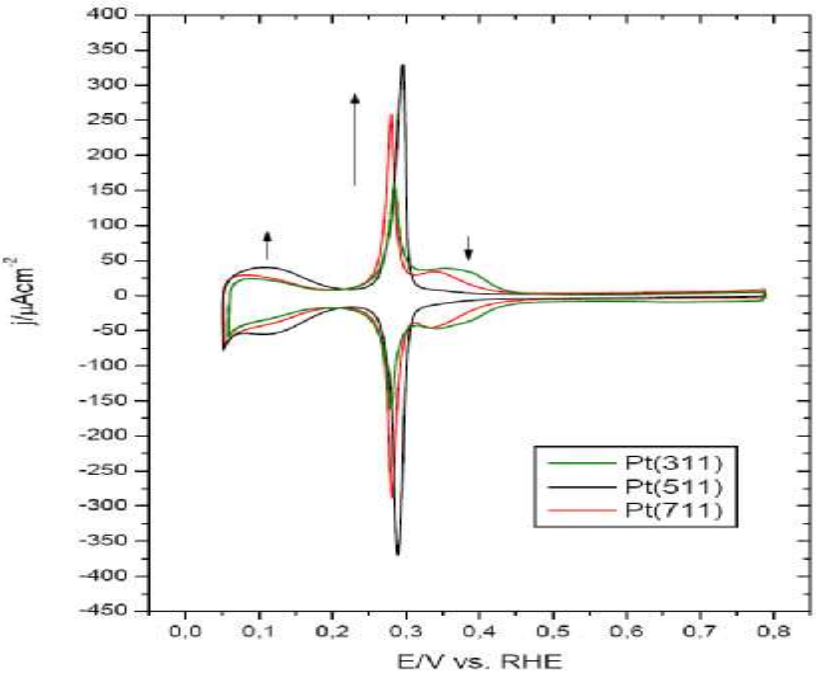


Figure 2.21. The CVs of Pt stepped single crystals Pt(S)[n(100)x(111)] with n= 2 , 3 and 4 with v = 50 mV/s .

2.5. CV measurements

CV techniques are easy to use and produced useful information about oxide thickness. To gain good results it is necessary to avoid every kind of contamination of the cell parts and the solution, which would be directly visible in the voltammograms. In order to prove that the solution is clean enough for further experiments, before each experiment a CV of well known basal plane was measured (Pt (111) or Pt (100)) [F. Hernandez and H. Baltruschat, (2006)].

2.6. Under potential deposition (UPD)

The adsorption and deposition of metal atoms on foreign metal substrates represents a very attractive family of systems for study because the strong adatom/substrate bonding can control the growth behavior and the resulting structures, especially as a function of surface coverage. Particularly attractive is the study of such systems by electrochemical means, especially within the context of underpotential deposition (UPD).

Underpotential deposition (UPD) species at a potentail less negative than the Nernst equilibrium potential for the reduction of this metal.The occurance of underpotential deposition is generally explained as a result of strong interaction between the electrodepositing metal with the substrate. The interaction between the metal and substrate needs energetically favoured to the metal-metal interaction in the crystal lattice of the pure metal.

A metal deposition from a metal salt solution on an electrode surface often can proceed at a potential, which lies above the thermodynamic potential of the regarded process. This phenomenon is caused by strong interactions between substrate and adsorbate. The equilibrium potential by the Nernst equation [R. Francke, (2008)].

$$P_0 = \rho_{00} + RT/ Z.F \ln a_{M+Z}$$

where ρ_0 is the Nernst potential, ρ_{00} the standard potential, z the number of transferred electrons and a_{M+Z} the activity of metal ions in solution.

In order to understand the under potential deposition, one has to distinguish between the properties of a monolayer and the bulk metal. In the thermodynamic consideration the chemical potential of the monolayer μML is lowered in comparison to the chemical potential of the bulk metal μM, due to interactions between the electrode surface and the deposited atoms.

2.7. Electrode Immersion Technique

In this method, the flame-annealed Pt electrode protected by a droplet of water was immersed in the aqueous metal solution for a fixed length of time to produce an overlayer of the desired metal coverage. Any excess of metal solution was then rinsed off and the electrode was transferred to the electrochemical cell as usual. The immersion in the same metal cation solution could be repeated many times in order to increase the number of adatoms. One could also simply increase the time of exposure of the single crystal to the metal cation solution. However, it was found that a much more controlled method of deposition using immersion was to use different concentrations of metal ion. Finally, after completion of all metal deposition experiments, the platinum crystal was removed from the solution and etched in nitric acid to dissolve away any residual surface adatoms prior to flame-annealing in order to avoid the possibility of forming an alloy.

2.8. CO oxidation

Carbon monoxide is one of the best characterized adsorbates in catalysis because of its specific role in many catalytic reactions. Since it is a strongly adsorbed species, it usually blocks the catalyst's surface for desired reactions.

In the electrochemical environment, the oxidation of pre-adsorbed CO is known to proceed through a two-step (Langmuir-Hinshelwood) mechanism. The first step involves the adsorption of OH, while, in the second step, the adsorbed OH causes oxidation of CO;

$$H + 2O + * \rightarrow OH_{ad} + H^+ + e^-$$

$$OH_{ad} + CO_{ad} \rightarrow 2* + CO_2 + H^+ + e^- \qquad \text{[H. A. Gasteiger, (1993)]}$$

where * denotes an empty site on the metal. On Pt, the rate-determining step is the first reaction, as electro-oxidation starts as soon as OH adsorption sets in. However,

the second step appears to be the rate-determining one on Ru, as the metal's surface is covered with OH_{ad} very early in the potential scale, before the onset of oxidation.

2.9. AIM OF THIS WORK

The aim of these experiments is to study adsorption of various metals on stepped surfaces with (100) terraces. Whether these metals can decorate on the steps or terraces. It is worked with Tl, Pb and Ru in this experiment. They are just an example of metal adsorption or the deposition of monolayer on Pt surfaces.

2.9.1. Why Thallium and Lead?

In literature there are not many article about the adsorption of these metals on Pt surfaces. Copper and some of the other metals were examined before and we have an idea about these metals, but not for thallium and lead. I wanted to have deposition monolayer in the potential range between 0 and 1.0 V. It can be adsorbed and desorbed this metals in this potential range. This is only possible for this metals [N. Bogolowski, (2008)].

2.9.1.1. Thallium

Chemical element, metal of main Group 13 of the periodic table .When freshly exposed to air, thallium exhibits a metallic lustre, but soon develops a bluish-grey tinge, resembling lead in appearance. A heavy oxide builds up on thallium if left in air, and in the presence of water the hydroxide is formed. The metal is very soft and malleable. It can be cut with a knife.

The element and its compounds are toxic and should be handled carefully. Thallium may cause cancer [Gary Attard, (1998)].

Symbol: Tl
Atomic number : 81
Atomic weight: 204.3833 (2)
Standard state: Solid at 298 K

Atomic Structure of Thallium

Atomic Radius: 2.08 Å
Atomic Volume: 17.2cm^3/mol
Covalent Radius: 1.48Å
Cross Section : (Thermal Neutron Capture) σ_a/barns**:** 3.43
Crystal Structure: Hexagonal

Uses of Thallium:

Its compounds are used in rat and ant poisons. Also for detecting infrared radiation and heart muscle research.

2.9.1.2. Lead

Lead is the heaviest member of the carbon family. The carbon family consists of the five elements in Group 14 (IVA) of the periodic table. Lead is known to be a poisonous metal that is able to bring about blood and brain disorders and can cause an effect on the nervous connections in the body. Element lead can be found in concentrations in the crust of the earth, however, element of lead does not form crystals on its own and therefore the mineral lead is not seen that often.

Symbol : Pb
Atomic number :82
Atomic mass : 207.2

The Physical Properties of Lead

Color: Light gray to a slight bluish grey color
Hardness: 1.5
Streak: Light gray and has a shiny streak
Transparency: Opaque
Specific gravity: 11.3
Luster: Metallic
Cleavage: No cleavage
Fracture: Hackly
Density: 11.4 qm.cm^3

Physical properties

Lead is a heavy, soft, gray solid. It is both ductile and malleable. Ductile means capable of being drawn into thin wires. Malleable means capable of being hammered into thin sheets. It has a shiny surface when first cut, but it slowly tarnishes (rusts) and becomes dull. Lead is easily worked [Gary Attard, (1998)].

Chemical properties

Lead is a moderately active metal. It dissolves slowly in water and in most cold acids. It reacts more rapidly with hot acids. It does not react with oxygen in the air readily and does not burn.

2.9.2. Why Ruthenium?

Catalysts of Pt group metals are of technological importance and are used indispensably in modern chemical industry, petrochemical industry and fuel cells, owing to their excellent activity and stability.

In alloys with Pt, Ru has a good catalytic properties for the CO oxidation in fuel cells. Ruthenium is often studied on Pt single-crystal surface with defined surface geometry. For preparation process after heating and cooling in a hydrogen atmosphere process it can be modified with Ru by potential controlled adsorption from a ruthenium containing solution. But ruthenium single-crystals are harder to prepare because they are oxidized by oxygen [N. Tian, (2008)] [B. Lanova, (2009)].

2.9.2.1. Ruthenium

Physical Properties of Ruthenium

Atomic Mass Average: 101.07
Boiling Point: 4173K 3900°C 7052°F
Coefficient of lineal thermal expansion/K^{-1} : $9.1E^{-6}$
Conductivity
Electrical: 0.137 10^6/cm Ω
Thermal: 1.17 W/cmK
Density: 12.37g/cc at 300K

Description:

Ruthenium is a hard, white metal. It does not tarnish at room temperatures, but oxidises in air at about 800°C. The metal is not attacked by hot or cold acids or aqua regia, but when potassium chlorate is added to the solution, it oxidises explosively.

Uses of Ruthenium

Used to harden platinum. Also used in eye treatments, thickness meters for egg shells, fountain pen points, and electrical contacts. Aircraft magnetos use platinum alloy with 10% ruthenium [B. Lanova, (2009)].

3. LITERATURE SURVEY

3.1. Adsorption Test

This is for cleaning the polycrystaline platinum electrode.

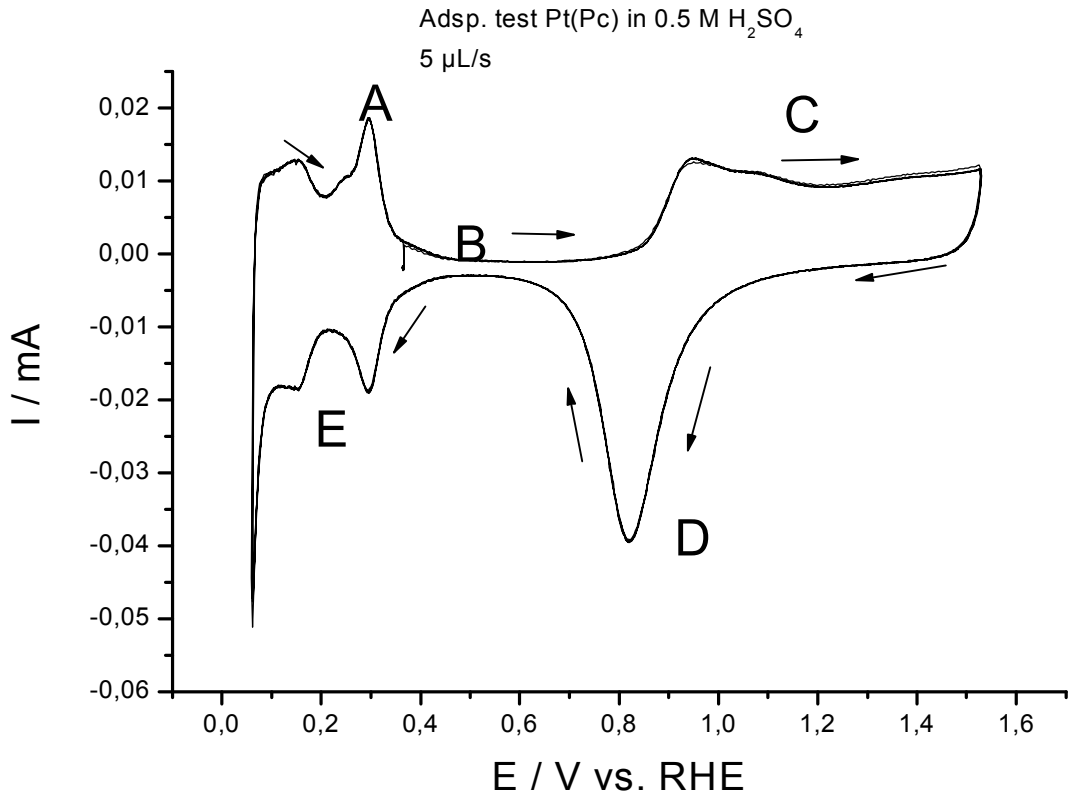


Figure 3.1. Scheme of adsorption test.

At section A is desorption of hydrogen from the platinum surface. The hydrogen adlayer is desorbed in two steps, the reactions being the reverse of those presented above.

$$H_{(ads)} \rightarrow H^+_{(aq)} + e^-$$

At section B there is no current flows in the system, this point is double layer.

At section C ; at nearly 0.8V the adsorption of an oxygen species to form a Pt surface oxide is under way. Oxygen-containing species become strongly chemisorbed and eventually may enter into the bulk.

$$Pt + H\text{-}O\text{-}H \rightarrow Pt\text{-}O\text{-}H + H^+ + e^-$$

$$Pt\text{-}O\text{-}H + H\text{-}O\text{-}H \rightarrow Pt\text{-}(OH)_2 + H^+ + e^-$$

$$Pt\text{-}(O\text{-}H)_2 \rightarrow Pt\text{-}O + H\text{-}O\text{-}H$$

At section D is PtO reduction in cathodic direction at nearly 1.2 V.

$$Pt\text{-}O + 2H^+ + 2e^- \rightarrow Pt + H_2O$$

At section E a hydrogen layer is adsorbed onto the surface in two distinguishable stages.

$$Pt + H^+ + e^- \rightarrow Pt\text{-}H_{(ads)}$$

3.2. Hydrogen adsorption on the low-indexed Pt single-crystals and on stepped single-crystals vicinal to the (100) surface in sulphuric and perchloric acid.

The cylic voltammogramms of the low-indexed Pt single-crystals and stepped Pt single-crystals vicinal to the (100) surface show charcteristic peaks for the adsorption and desorption of hydrogen and a clear trends for these peaks is visible, when the surfaces are stepped, especially in sulphuric acid. The voltammograms of these surface are like “finger-prints”, and they can be used to identify the single-crystals or to judge about a succesful preparation of the surface.

Figure 3.2. Reprinted from Bogolowski et al , [N. Bogolowski, (2008)] shows the CVs for the three Pt single crystals Pt (100), Pt (110) and Pt (111) in 0.1 M H_2SO_4 with a sweep rate of 50 mV/s which could be considered as ideal infinitely wide terraces of the basal planes. The charge density in the potential range between 0 and 400 in the CV for the Pt (100) is related to hydrogen adsorption/desorption. The

peak for strongly bound hydrogen at the more positive potential of 0.35 V in the anodic scan has been attributed by Clavelier et. al. [J. Clavilier and D. Armand, (1986)] to hydrogen desorption from flat (100) terraces, whereas the peak at 0.24 V is related to hydrogen adsorption at defect sites. The peak in the CV for Pt(110) at a potential of 0.07 V is related to hydrogen adsorption/desorption. Whether this is on the reconstructed or on the (1x1), is indistinguishable from the CV in sulphuric acid [R. Michaelis and D. M. Kolb, (1992)] [R. Michaelis, (1992)]. For the Pt(111) in the potential range between 0 and 0.35 V vs Pd/H mainly hydrogen is adsorbed/desorbed. The small peaks at 0.07 and 0.22 V are related to hydrogen adsorption/desorption on defect sites [J. M. Feliu, (1994)] [A. M. Funtikov, (1995)].

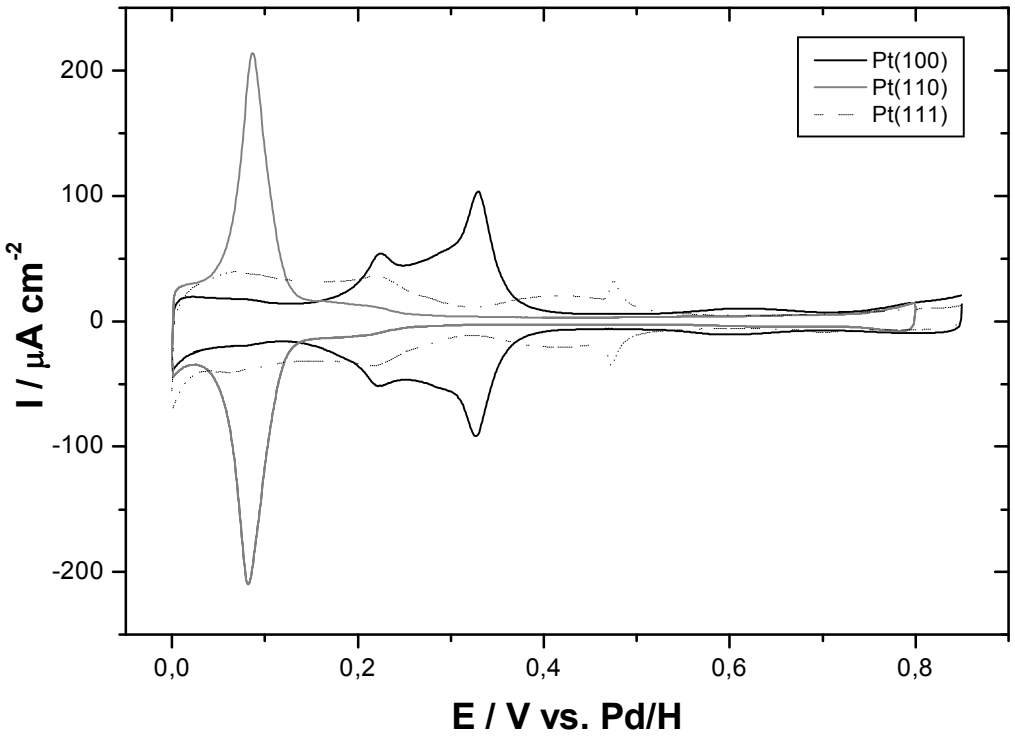


Figure 3.2. Voltammetric profiles of the low-indexed Pt (100), Pt (110) and Pt (111) single-crystal surfaces in 0.1 M H_2SO_4 v= 50 mV/s [N. Bogolowski, (2008)].

Figure 3.3. Reprinted from Bogolowski et al [N. Bogolowski, (2008)] shows the CVs for the stepped Pt(S)[n(100)x(111)] single-crystals surfaces with a terrace-

width n = 2, 4 and 6. In the potential region between 0 and 0.40 V is related to hydrogen adsorption/desorption.

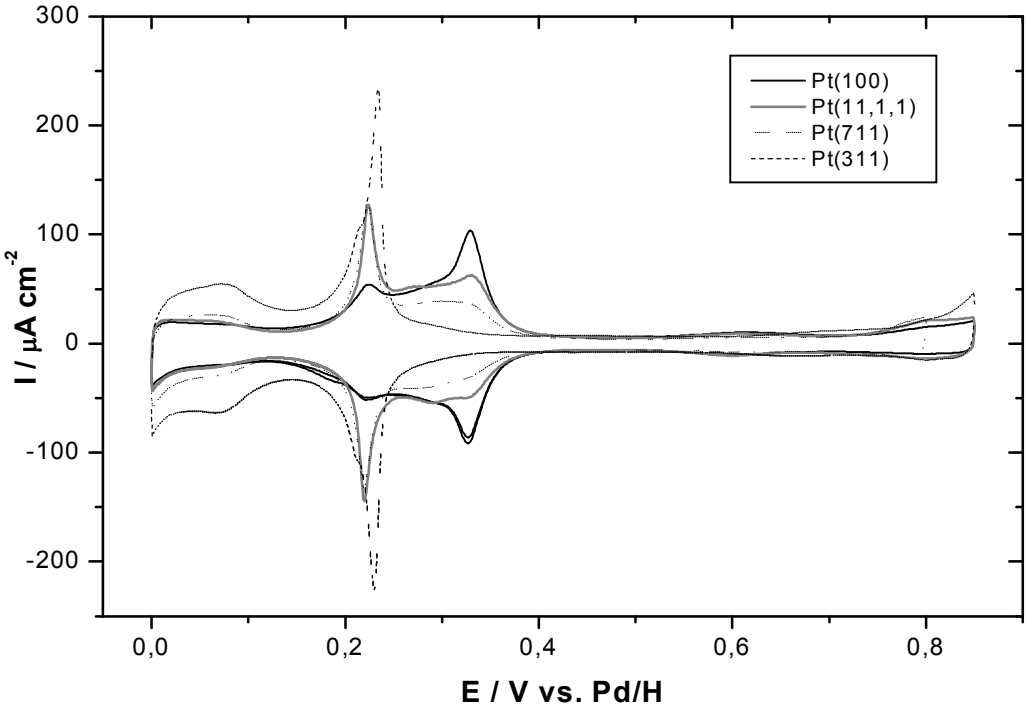


Figure 3.3. Voltammetric profiles of the low-indexed Pt (100) and Pt(S)[n(100)x(111)] electrodes with n = 2 , 4 , 6 in 0.1 M H_2SO_4 v= 50 mV/s [N. Bogolowski, (2008)].

The voltammogramms of the low-indexed Pt single-crystals and stepped Pt single-crystals vicinal to the (100) surface which recorded in perchloric acid are not as characteristic as the ones in sulphuric acid, only the CVs of the low-indexed surfaces differ drastically. Nevertheless, even in perchloric acid, a clear trend for the influence of steps on the surfaces vicinal to the (100) surface is visible.

Figure 3.4. Reprinted from Francke et al [R. Francke, (2008)] the blank voltammograms of the Pt(S)[n(100)x(111)] electrodes, with n = 3, 4, 8, 20 and Pt(100) in 0.1 M perchloric acid with sweep rate v=50 mV/s are shown. They resemble the shape and peak intensity is used in this work to control the preparation of the Pt single-crystal. The voltammetric profiles look different from those recorded in 0.1 M sulphuric acid, but still contain the important peaks with almost the same

assignment. According to Francke et al [R. Francke, (2008)], instead of a competitive hydrogen/anion adsorptionat potentials underneath 0.5 V hydrogen adsorption is dominant, while this process is superimposed with OH-adsorption at potentials higher than 0.5 V, all due to the fact that the perchlorate anion does not adsorb significantly at Pt surfaces within the applied potential region.

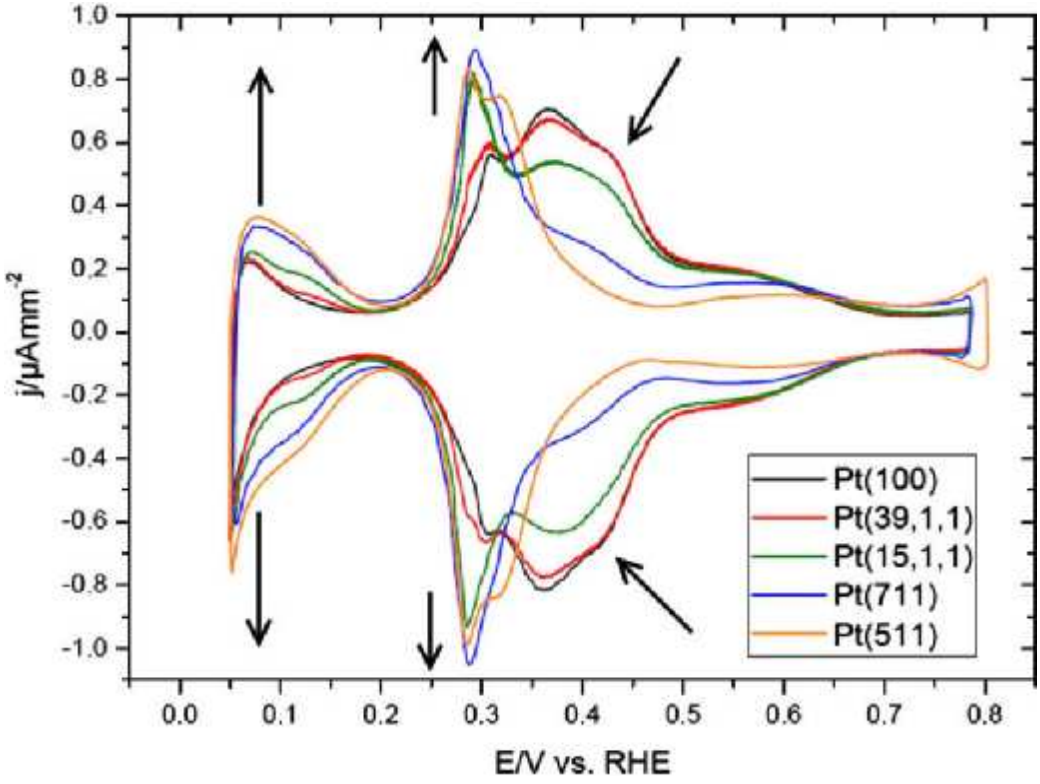


Figure 3.4. Voltammetric profiles of the Pt(S)[n(100)x(111)] electrodes, with n = 3, 4, 8, 20 and Pt(100) in 0.1 $MHClO_4$ v = 50 mV/s. Arrows indicate the increase of the step density. Reprinted from [R. Francke, (2008)].

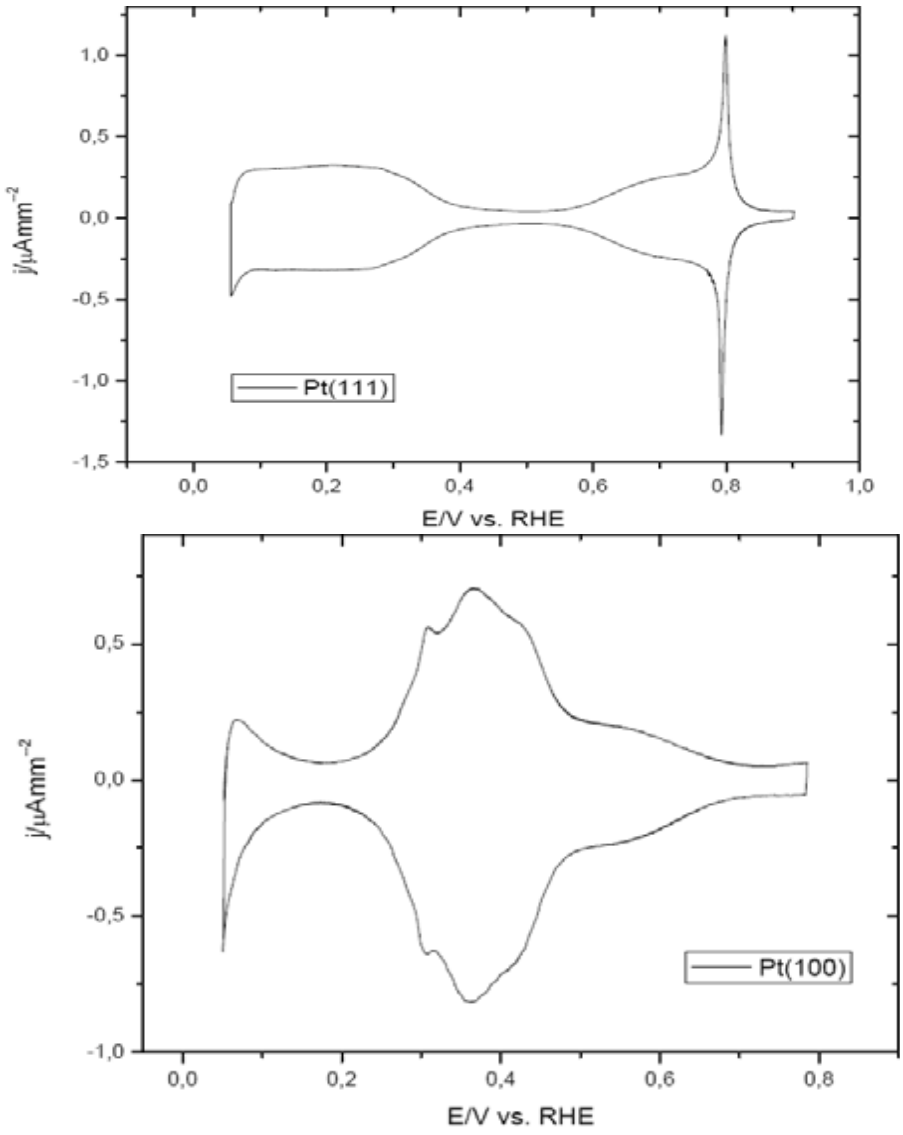


Figure 3.5. Cyclic voltammograms of the basal planes Pt(111) and Pt(100) in 0.1 M $HClO_4$, v = 50 mV/s. Reprinted from [R. Francke, (2008)].

3.3. Tl and Pb UPD

The typical voltammogram of the underpotential deposition and desorption of Tl^+ in 0.5 M H_2SO_4 solution as supporting electrolyte on a Pt (111). At low potential, all the sites of the surface are blocked for the reversible adsorption of the weakly bonded hydrogen. II and III peaks are related to central region of the voltammogram. At the high potential it contains a pair of slightly irreversible sharp peaks I_c and I_a.

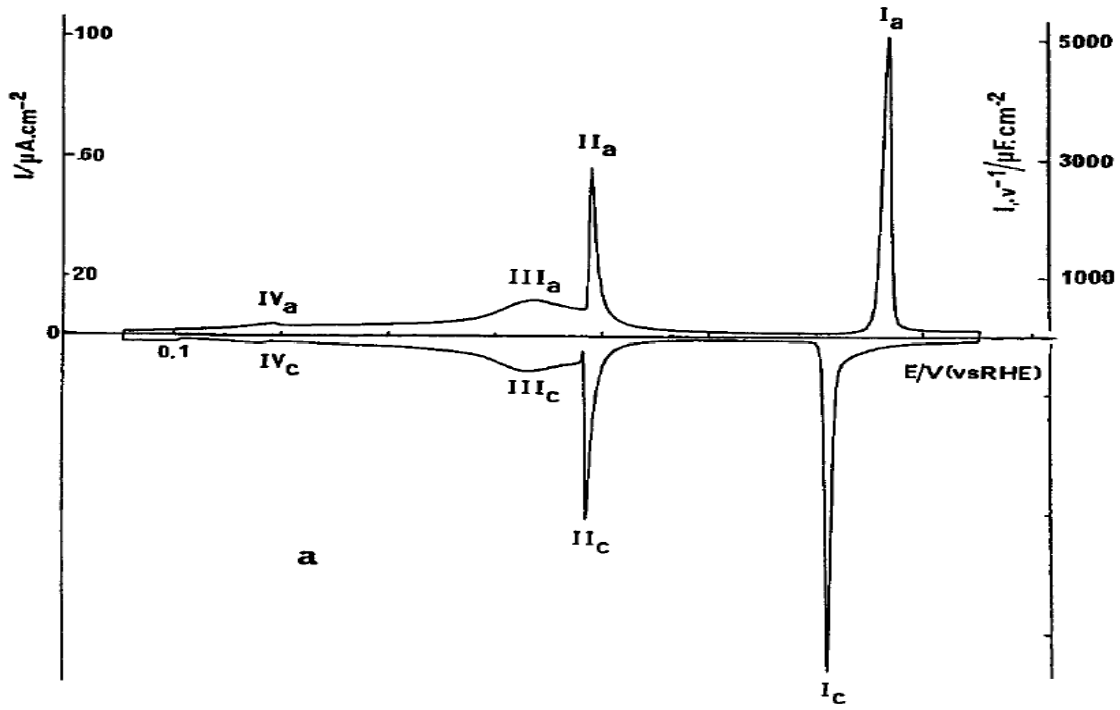


Figure 3.6. Voltammogram of a Pt (111) orientated electrode in contact with an acidic solution of thallium, $5x10^{-3}$ M Tl^{+} in 0.5 M H_2SO_4; v= 20 mV/s. Reprinted from [J. Clavilier, (1989)].

The effect of the UPD of Pb on the voltammetric features of Pt (100) recorded in pure 0.1 M $HClO_4$ is easily observed simply by comparing the voltammetry of Pt (100) with and without Pb^{+2} as shown below the figure. 3.7.a) reveals that information of a monolayer of hydrogen in 0.10 M $HClO_4$ occurs through two distinctive small voltammetric peaks, the first at 0.10 V and second at 0 V. These two peaks most likely correspond hydrogen adsorption/desorption on (100) terrace sites and on (100)x(111) terrace-step sites.

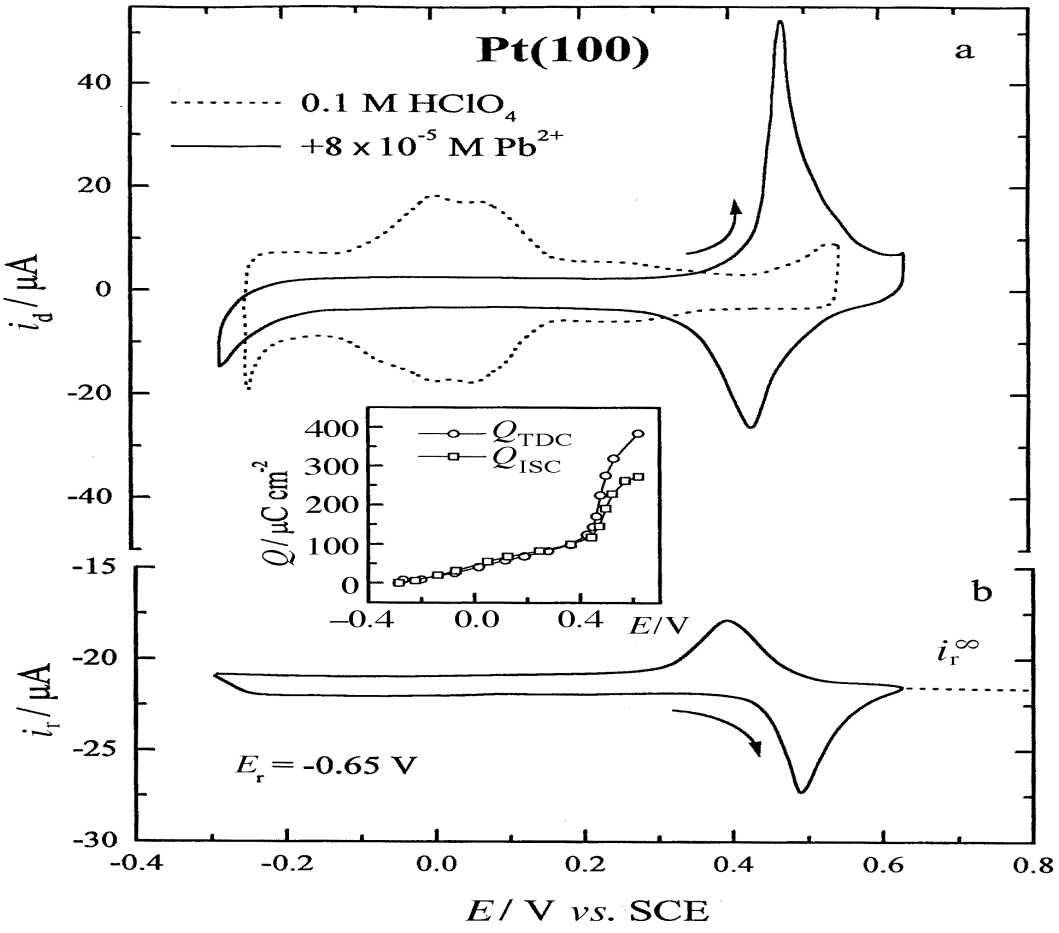


Figure 3.7. (a) Cyclic voltammogram for Pb UPD in 0.1 M HClO4 on the Pt (100) disk electrode in a RRDE assembly. Base voltammogram without Pb^{+2} in solution under otherwise identical conditions is shown for comparison. (b) Ring electrode current with the ring being potentiostated at 0.65 V. Insert: Integrated charges for the stripping of Pb from the disk electrode assessed from ring (ISC) and disk (TDC) uppdotentiodynamic curves. Rotation rate 900 rpm; sweep rate 50 mV/s.

The cyclic voltammograms of Pt (111) in 0.1 M $HClO_4$ free of lead, and in the presence of $5x10^{-5}$ M Pb^{+2} are shown in below the figure 3.8. The CV shows a characteristic broad hydrogen adsorption wave, -0.22 < E < 0.1 V, and the so-called "butterfly peak" at 0.3-0.6 V, which corresponds to adsorption of hydroxyl species.

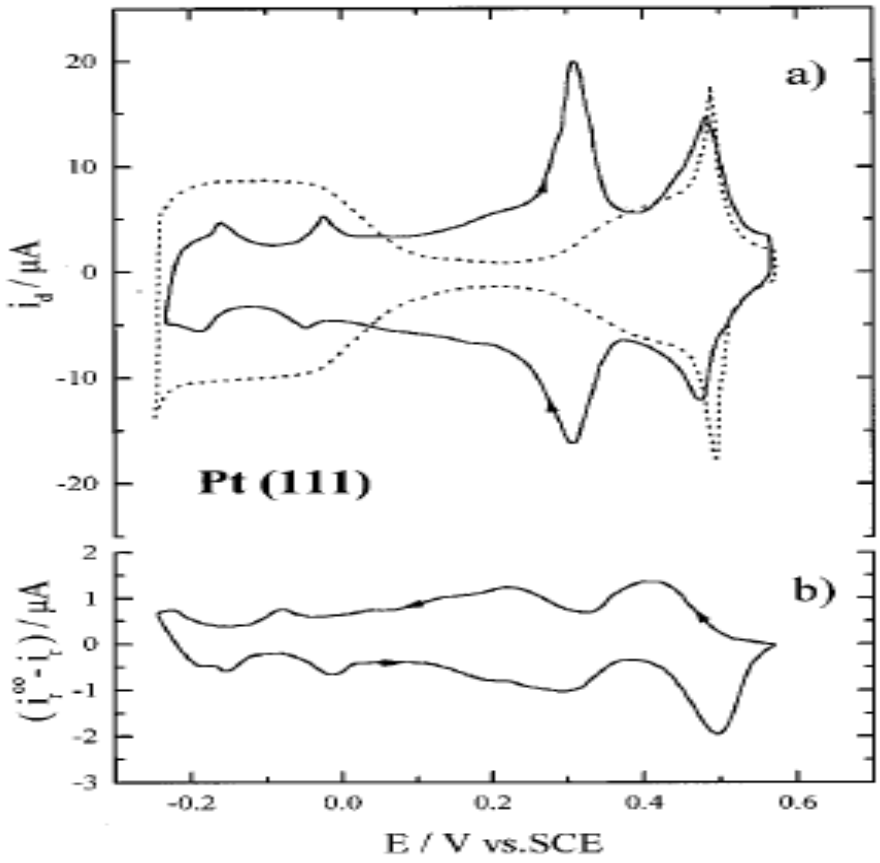


Figure 3.8. a) Cyclic voltammograms of Pt(111) mounted in the disk position of the RRDE in 0.1 M $HClO_4$ and $5x10^{-5}$ M Pb^{+2} : rotation rate , 900 rpm ; sweep rate , 50 mV/s b) Ring electrode currents recorded with the ring being potentiostated at -0.59 V.

3.4. Effect of Ru deposition on the CO oxidation at Pt single-crystals

The sequence of deposition of Ru has a minor influence on the shape of the mass spectrometric cyclic voltammograms. The onset of CO oxidation is lowered to similar values as on the corresponding Pt-surfaces modified by Sn alone, which is much lower than achieved by modification with Ru alone.

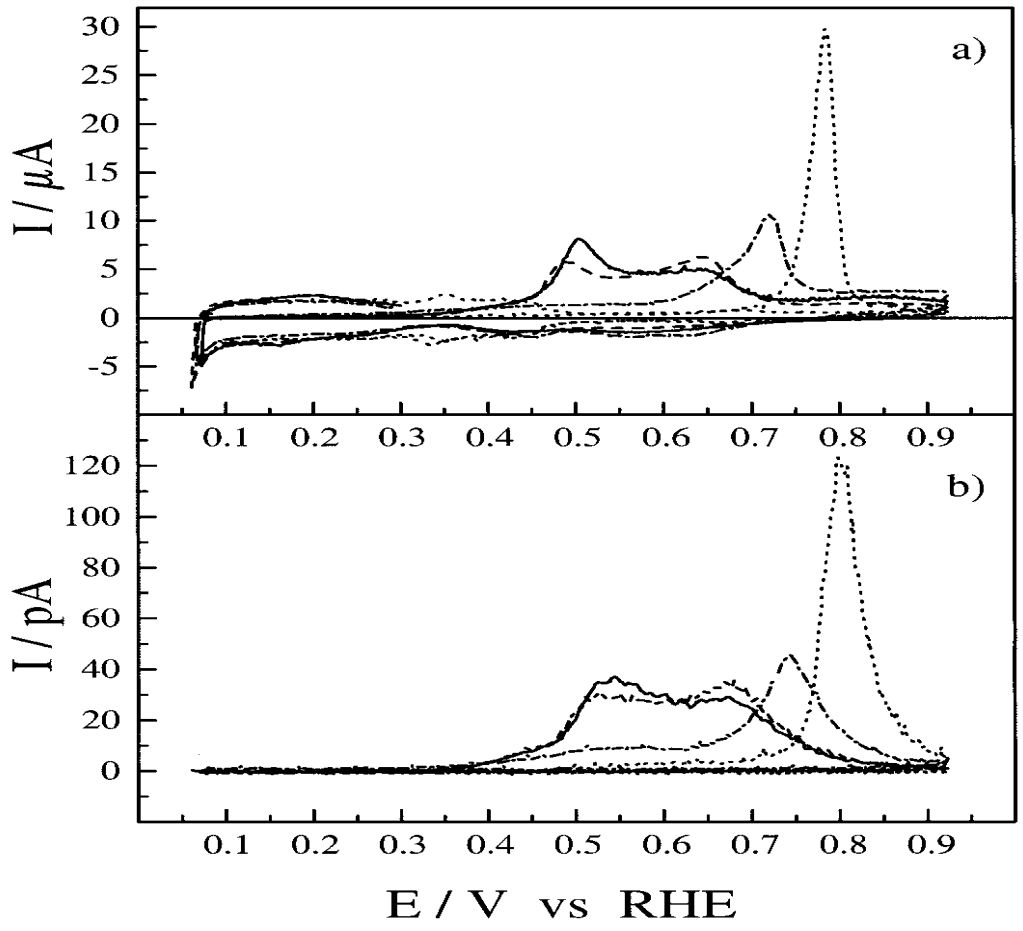


Figure 3.9. Shows the CV of oxidation of adsorbed CO at Pt(111) covered by (submonolayers of) Ru and Sn. CVs are shown in 3.9.a) ; MSCVs (mass spectrometry cyclic voltammetry) for CO_2 are shown in 3.9.b) dE/dt=10 mV/s , 0.5 M H_2SO_4 (__) deposition of Ru followed by deposition of Sn (- - -) deposition of Sn followed by deposition of Ru(-.-.-) only deposition of Sn(…) bare Pt-surface for comparison. Reprinted from [H. Massong, (2000)].

4. MATERIALS AND METHODS

4.1. Materials

4.1.1. Chemicals

Table 4.1. The chemicals that used in this work.

Name / Formula	**Description / Company**	**Typical Use**
Sulphuric acid **H_2SO_4**	% 95-97 Aldrich	Base electrolyte
Perchloric acid **HCl_4**	% 70 Aldrich	Base electrolyte
Ruthenium (III) chloride **$RuCl_3$**	Aldrich	Electrolyte for Ru deposition
Lead (II) perchlorate **$Pb(ClO_4)_2$**	% 99 Aldrich	Electrolyte for Pb deposition
Thallium (I) sulfate **Tl_2SO_4**	% 99 Aldrich	Electrolyte for Tl deposition
Potassium hydroxide **KOH**	Aldrich	Tip etching solution
Platinum **Pt** wire	ChemPur GmbH 0.5 mm diameter	For Pt single-crystals
Argon **Ar** (Gases)	Praxair 5.0	Degassing of the electrolyte and preparation of single crystals
Hydrogen **H_2** (Gases)	Praxair 6.0	Preparation of single crystals

The Milli-Q-Water System

In this work the Milli-Q plus system (Millipore, Watford, Hertfordshire) is used to produce ultra-pure water which contained very low levels of organic material. The system is capable of producing up to 1.5 litres per minute of ultra-pure 18.2 MΩ cm receptivity water with a total organic content of less than 10 parts per billion. Ultra-pure water is used for cleaning glassware and for the preparation of all electrolyte solutions.

4.1.2. Apparatus

• An electrochemical cell with the cell accessories (hydrogen reference electrode platinum counter electrode, Teflon crystal holder and gas caps)
• A variety of glassware (beakers, measuring cylinders, volumetric flasks, pipettes and gases bubblers)
• A series of platinum single crystal electrodes

4.1.3. The Bead Single Crystal Teflon-Holder

The single-crystal holder has two steel rods for electrode contact inside the Teflon-holder. The Teflon holder can be easily moved up and down . The single-crystal itself was contacted via two small Pt-wires, one wrapped around the end of the Pt wire where the crystal was made of, the other at the beginning of the bead single-crystal , to screw holes at the end of the steel rods. This setup allows easily varying the distance between the crystal surface and solutions to have a good hanging meniscus-configuration and resistive heating of the crystal [N. Bogolowski, (2008)].



Figure 4.1. The Pt-electrodes with Teflon-holder.

4.1.4. Electrochemical Instrumentation

4.1.4.1 The Electrodes

a) Working electrodes

I studied with Pt electrodes as a working electrodes. For quantitative electrochemical analysis in laboratories; Platinum electrodes of various types are used in this work.

• Flat single crystals: Pt (111) and Pt (100)

• Stepped single crystals: Pt (511) , Pt (11,1,1) , Pt (19,1,1)

Why platinum?

Platinum is a lustrous, silvery-white, malleable and ductile metal. It is unaffected by air and water, and will only dissolve in aqua regia and molten alkalis

[A. M. Bittner, (1997)]. There are a lot of reasons for choice of platinum for the hydrogen electrode :

♦ Inertness of platinum (it does not corrode)
♦ The capability of platinum to catalyze the reaction of proton reduction
♦ A high intrinsic exchange current density for proton reduction on platinum (see the data in the table for comparison of platinum with other materials)
♦ Excellent reproducibility of the potential (bias of less than 10 μV when two well-made hydrogen electrodes are compared with one another.

Melting Point : 1772 °C
Lattice Constant : 3.9231 Å
Atomic Diameter : 2.774 Å

b) Reference electrodes and Counter electrodes

In this work it is used hydrogen electrode as reference electrode and a platinum electrode as counter electrode. To keep it free from contamination, it was stored in 0.1 M H_2SO_4 for thallium and ruthenium experiments and in 0.1 M $HClO_4$ for lead experiments.

A reference electrode is an electrode which has a stable and well-known electrode potential. The high stability of the electrode potential is usually reached by employing a redox system with constant (buffered or saturated) concentrations of each participants of the redox reaction.

Reference electrodes, as their name suggests, are used to give a value of potential to which other potentials can be referred in terms of a potential difference—potentials can only be registered as differences with respect to a chosen reference value. Thus, a good reference electrode needs to have a potential that is stable with time and with temperature and which is not altered by small perturbations to the system—that is, by the passage of a small current. There are three types of reference electrode:

• *Type 1:* e.g. the hydrogen electrode
• *Type 2:* e.g. the calomel electrode
• *Others:* e.g. glass electrodes, Type 3 electrodes, etc.

The reference electrode is used in the H-cell experiments is a reversible hydrogen electrode (RHE) in 0.1 M H_2SO_4 and $HClO_4$. In principle, vacuum is applied to the open arm of the glass cylinder to fill the bulb of the electrode with electrolyte. The electrode is then connected to the negative terminal of a dc power supply (10-20 V) using a Pt wire as the counter electrode, in the same electrolyte. Pt wire was briefly immersed in concentrated HCl to remove traces of foreign metals and oxide, then flame-annealed for a few seconds.

Due to the electrolysis of the sulphuric acid solution, hydrogen is generated on the negative electrode, while oxygen evolves from the counter electrode. The hydrogen bubble displaces the solution inside of the bulb, creating a gas/liquid interface in contact with the Pt wire. This vacuum and electrolysis procedure is repeated one more time in order to make sure that the bubble trapped in the bulb is pure hydrogen without traces of atmospheric oxygen. The electrode is stored in the glass cylinder, keeping the bulb immersed in electrolyte. Fresh reference electrodes must be prepared often and handled with care to avoid variations in the potential due to atmospheric oxygen entering the bulb.
Hydrogen electrode is based on the redox half cell.

$2H^+(aq) + 2e^- \rightarrow H_2(g)$

This redox reaction occurs at platinized platinum electrode. That implies that the pressure of hydrogen gas is 1 bar and the concentration of hydrogen in the solution is 1 molar. The Nernst equation should be written as: Equation is taken from [R. Francke, (2008)].

$$E = \frac{RT}{F} \ln \frac{a_{H^+}}{(p_{H_2}/p^0)^{1/2}}$$

or

$$E = -\frac{2.303RT}{F}pH - \frac{RT}{2F}\ln p_{H_2}/p^0$$

4.1.4.2 The Cell

The cell is made of borosilicate glass and consists of three sections; the body of the cell, one compartment for the reference and one for the counter electrode.

The body of the cell has room for the working electrode and the electrolyte. A glass tube coming from the back part of the cell can be used as inlet to bubble gas in the electrolyte. A stopcock allows to adjust precisely the electrolyte level.

The reference electrode compartment is connected to the cell body with a Luggin capillary. Since there is a stopcock separating them, different solutions can be used in both chambers; this is advantageous when working with electrolytes containing metal ions which could contaminate the reference electrode. The stopcock is made of glass, and thus hydrophilic. The thin layer of electrolyte wetting the glass has sufficient conductivity to keep potential control even if the stopcock is closed. A fritted glass disk separates the counter electrode compartment from the main room of the cell.

4.1.4.3 The Potentiostat

In this work it is used Potentiostat / Galvanostat Model 273.It is for use with Solartron 1260 EIS-Analyzer. This model has :

♦ High Sensitivity, Low Noise Signals
♦ High Speed Current Measurement
♦ Easy Front Panel Operation
♦ GPIB and RS232 Interfaces
♦ Many Advanced Features



Figure 4.2. Potantiostat/Galvonostat Model 273

4.1.5. Glassware

First of all, in my work cleaning is the most important thing. All the glassware must be very clean and degreased before every experiment. Cleaning with water is not enough.To dispose of traces of metal ions, the glassware is soaked overnight in chromic acid (640 ml of concentrated H_2SO_4 + 360 ml H_2O + 21.4 g CrO_3) at room temperature. Chromic acid generally refers to a collection of compounds generated by the acidification of solutions containing chromate and dichromate anions or the dissolving of chromium trioxide in sulphuric acid**.** After that, it is rinsed widely with Millipore water and stored in 5 M KOH solution to keep it free from grease. If the glassware is not contaminated metal ions or organic molecules, it is not important to soaked in chromic acid.

Cleanliness can be checked with a simple adsorption experiment using a Pt electrode before the main experiment. The Pt electrode is cycled several times in the electrolyte. When obtaining a steady CV, the potential is stopped in the double-layer region and kept there for a few minutes. After that, the potential scan is continued in the cathodic direction.

4.2. Methods

4.2.1. Preparation of well-ordered noble metal single crystal surfaces

Explanations of measurements to get ease and not to be misleading, we should be able to prepare reproducibly well ordered surfaces for all basic electrochemical investigations. A well-ordered low-index surface must be atomically flat, having large terraces separated by monoatomic high [J. Clavilier, (1980)], [K. Sashikata, (1991)], [S.L. Yau, (1996)].

The small spherical single crystals, which are often used for the flame annealing and quenching method are usually prepared by melting one end of a high purity wire. A well-prepared bead consists of (111) facets in an octahedral configuration consists of large terraces, separated by monoatomic high steps [J. Clavilier, (1980)], [P. N. Ross and F. T. Wagner, (1984)] , [M. P. Soriaga, (1992)].

4.2.2. Calculation of Charge in Cyclic Voltammetry

Charge associated with a cyclic voltammetry could be determined by two methods:

• Manual technique of cutting and weighing the peaks and then taking the ratio of the peak weight to a rectangle of a known area and weight.

• the second method, which was employed in the present study, by using a computer program to calculate the charge.

In the second method, after displaying the cyclic voltammogram on a monitor, the area between two potential limits could be calculated automatically by computer which then converts this number to charge density.

5. EXPERIMENTAL RESULTS AND DISCUSSION

5.1. Tl UPD on Pt (111), Pt (100), Pt(11,1,1) and Pt (511)

5.1.1. Voltammetry of the unmodifed Pt bead single–crystal surfaces in H_2SO_4

The desired Pt bead single crystal is cleaned by potential cycling in the range between 0.05 V and 1.5 V in 0.1 M sulphuric acid, performing several electrolyte-exchanges at 1,5 V. Then the crystal is annealed in a bunsen-burner flame for 45 s to a pale red colour, and afterwards allowed to cool down in a hydrogen atmosphere over MilliQ-water. Protected by a droplet of hydrogen saturated MilliQ-water, the electrode is transferred to the H-cell. Electrolyte contact is performed under potential control in a hanging meniscus configuration. To control the success of the preparation of the single-crystal surface by annealing, a CV is recorded in a potential range between 0.05 V and 0.8 V in 0.1 M sulphuric acid and compared to those reported in literature, e.g. [R. Francke, (2008)], [N. Bogolowski, (2008)]. After a successful preparation, the electrode is transferred to another cell, protected by an argon saturated droplet of sulphuric acid, with a Tl or Ru containing electrolytes, where e.g. the Tl UPD on the surface is investigated. Before immersion to an electrolyte containing Pb, i.e. a lead containg perchlorate solution, the electrode surface is rinsed with water to wash away the sulphate from the surface, because Pb forms insoluble salts with sulphate.

Figure 5.1. Shows the CVs for the unmodified electrodes of Pt(100) and Pt(111) in 0.1 M H_2SO_4. At 0.38 V in the CV for the Pt (100) is related to hydrogen adsorption/desorption. The peaks at 0.30 V and 0.35 V are related to hydrogen adsorption at defect sites. According to literature , the hydrogen peak at 0.38 V should be sharper and higher [R. Francke, (2008)]. For Pt (111) the CV can be divided in two region. In first region in the potential range between 0.05 and 0.35 V vs. RHE hydrogen is adsorbed/desorbed .The small peaks at 0.10 V and 0.25 V are related to hydrogen adsorption/ desorption on defect sites [D. R. Wheeler, (1995)].In the second region in the voltammogram between 0.35 V and 0.50 V sulphate

adsorption takes place. The "spike" at 0.49 V in the voltammogram indicates a phase–transition within the sulphate adlayer [A. M. Funtikov, (1997)]. At the potential range between 0.65 V and 0.80 V in the CV contains a pair of slightly irreversible sharp peaks.

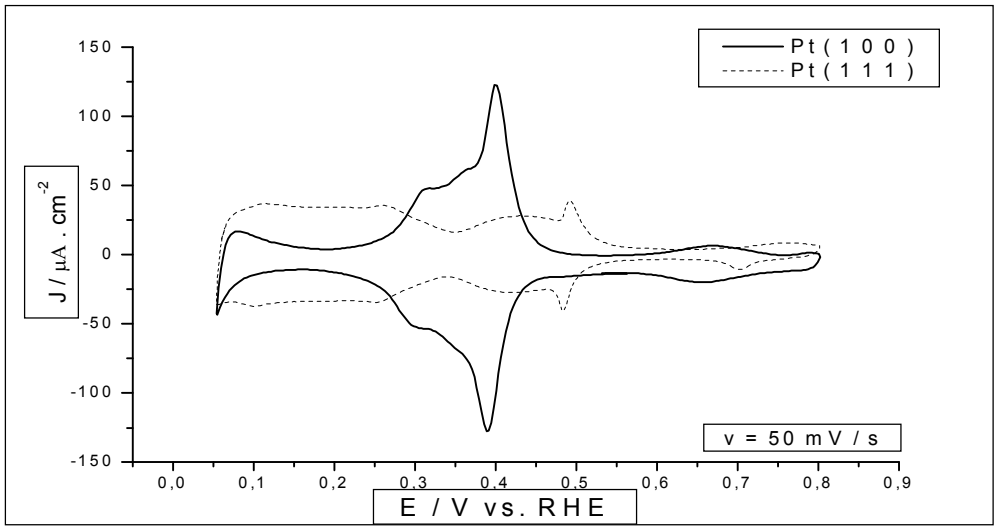


Figure 5.1. Recorded CVs of the two basal plane single-crystals in 0.1 M H_2SO_4 with v = 50 mV/s.

Figure 5.2. Shows the CVs for the unmodified Pt(S)[n(100)x(111)]-electrodes with n = 3 , 6 stepped single-crystal surfaces vicinal to the (100) surfaces and the CV for the Pt (100) surfaces in 0.1 M H_2SO_4. The potential range between 0.05 V and 0.17 V is related to hydrogen adsorption on step-sites with local (110) geometry. With increasing step-density on the Pt(S)[n(100)x(111)] surface, a clear trend for the sharp peak at around 0.25 V, assigned to hydrogen adsorption/desorption on the step sites, is visible. The charge-density of this peak increases with increasing step density.

For Pt (511) at the 0.29 V in the voltammogram is related to hydrogen adsorption and desorption peak at step sides.

For Pt (11,1,1) the sharp peak at 0.28 V , assigned to hydrogen/anion adsorption on the step sites in figure 5.2. In the same time, the peaks at potential around 0.40 V,

that is assigned to adsorption at terrace sites, decrease. As compared to literature the peaks for hydrogen adorption/desorption from step sites should be sharper [R. Francke, (2008)].

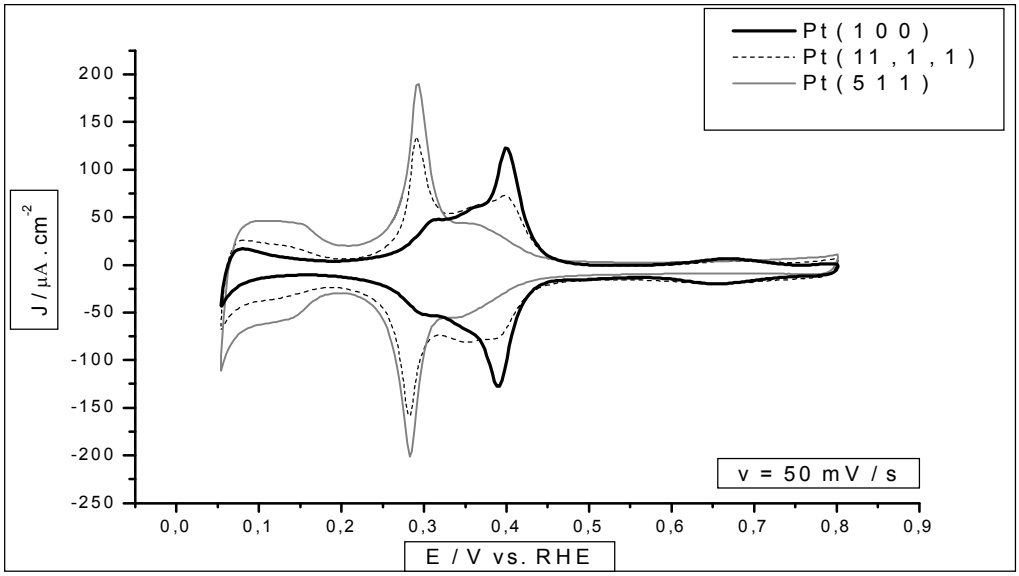


Figure 5.2. CVs of Pt stepped single crystals Pt(S)[n(100)x(111)] with n= 3 , 6 and Pt (100) in 0.1 M H_2SO_4 with v=50 mV/s.

For the CVs in figure 5.1. and 5.2. in the potential range of 0.10 V to 0.45 V a charge-density of these CVs are integrated after correction of double-layer contribuation and they are summarized in Table 5.1.

Table 5.1. Charge of various Pt-single crystals for the integration limit is between 0.10 and 0.50 V. For Pt (111) integration limit is between 0.10 and 0.45 V.

Single Crystal	**Charge / µC.cm^{-2}**
Pt (100)	≈221
Pt (111)	≈188
Pt (511)	≈302
Pt (11,1,1)	≈270

5.1.2. Diffusion controlled Tl UPD on Pt(111) , Pt(100) , Pt(511) and Pt(11,1,1)

After the recording a voltammogram of the as prepared electrode in the base electrolyte , the electrode is transferred into the containing $1x10^{-3}$ M or $1x10^{-6}$ M Tl_2SO_4 solution and a voltammogram is recorded in the second cell**.** The Pt (111) electrode is cycled in the thallium solution for more than fifty cycles.

The Figure 5.3 shows the typical voltammogram of the underpotential deposition and desorption of Tl^+ in $1x10^{-3}$ M Tl_2SO_4 on a Pt (111) electrode. According to Oda et al [I. Oda, (1996)] there is a strong suppression of the hydrogen-UPD region by adsorbed Tl in the potential range between 0.05 V an 0.35 V. The broad peak at positive potentials is related to the adsorption of sulphate and shows a sharp peak at 0.54 V which as in the case for the thallium free electrolyte is related to a phase transition in the sulphate-adlayer structure [A. M. Funtikov, (1997)].

The charge of this peak integration limit between 0.40 V and 0.60 V is ≈108 $\mu C.cm^{-2}$. The sharp irreversible peak pair at an anodic potential of 0.78 V and a cathodic potential of 0.76 V is according to Oda et al related to a phase-Transition from a $\sqrt{3}x\sqrt{7}$ - to a $\sqrt{3}x\sqrt{3}R30°$ -overstructure of the Tl-Adlayer after completion of the Tl-Monolayer. The charge of this peak at an anodic potential 0.78 V is ≈61 $\mu C.cm^{-2}$ and at an cathodic potential 0.76 V is ≈51 $\mu C.cm^{-2}$ which closed to theoretical value of ≈56 $\mu C.cm^{-2}$ and ≈50 $\mu C.cm^{-2}$ [J. Clavilier, (1989)] , [D. R. Wheeler, (1995)].

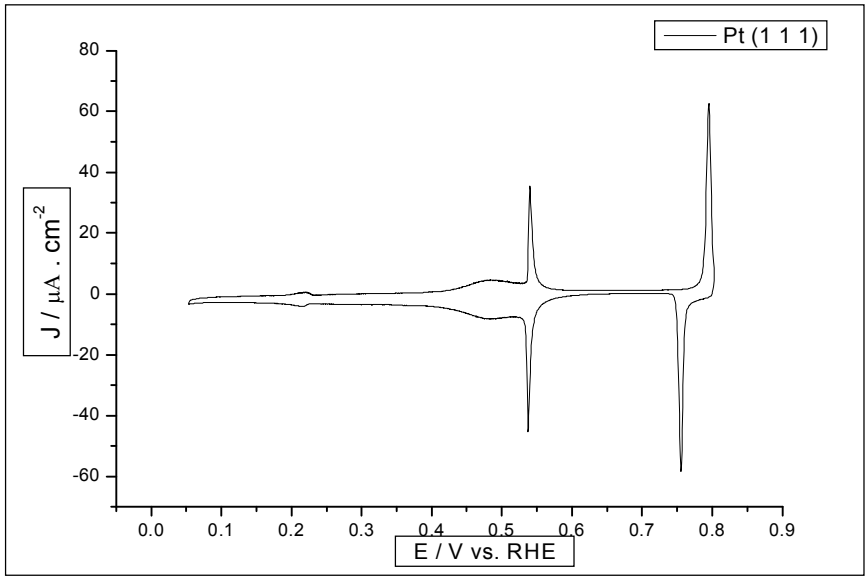


Figure 5.3. The CVs for Tl / Pt (111) in 10^{-3} M Tl_2SO_4 + 0.1 M H_2SO_4 with v=10 mV/s.

To test the cell setup, to train the electrode transfer and to have a comparison to the diffusion controlled Tl UPD experiments performed on the stepped single-crystal surface, firstly an experiment on the Tl UPD on Pt (111) is performed. And after that Pt (100) and stepped-crystals are performed.

Figure 5.4. Shows the voltammogram of the underpotential deposition and desorption of Tl^+ in $1x10^{-6}$ M Tl_2SO_4 solution on a Pt (11,1,1) electrode. After transferring the electrode from the base electrolyte, It cycled in the thallium containing solution for more than sixty cycles. Already in the first cycle, the sharp hydrogen adsorption peak at the 0.28 V and at the 0.40 V Tl dissolution. After sixty cycles it suppressed and the hydrogen adsorption peak shifted to the positive potential and the thallium peak height was decreased. In the potential range between 0.05 V and 0.17 V, the defect -sites are not totally suppressed. In the potential range between 0.50 and 0.80 V is related to sulphate sites. The charge of (111) step sites for Tl/Pt crystal is ≈126 $\mu C.cm^{-2}$ and for after preparation of Pt crystal is ≈140 $\mu C.cm^{-2}$. This is about 10% of the step-sites blocked by adsorbed Tl. The charge of (100) terrace-sites for Tl/Pt crystal is ≈135 $\mu C.cm^{-2}$ and for after preparation of Pt

crystal is ≈142μC.cm^{-2}. This is about 5% of the terrace-sites blocked by adsorbed Tl. It should be noted there integration limit for terrace in the potential range between 0.32 V and 0.48 V. For the charge results it seems to be there is no preferential on step-sites, whereas from the CV in figure 5.4. one can conclude that Tl preferentially adsorbs at step sites.

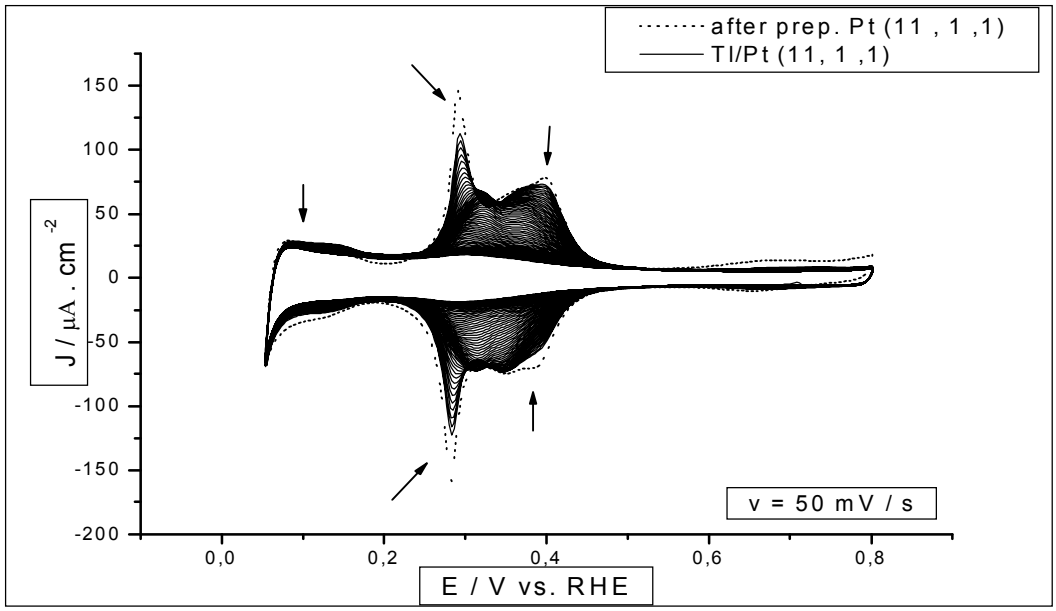


Figure 5.4. The CVs for Tl deposition (__) on Pt (11,1,1) in 1x10^{-6} M Tl_2SO_4 + 0.1 M H_2SO_4 and after preparation (. . .) with v= 50 mV/s.

Figure 5.5. Shows the voltammogram of the underpotential deposition and desorption of Tl^+ in 1x10^{-6} M Tl_2SO_4 solution on a Pt (511) electrode. It is cycled in the thallium solution for more than sixty cycles. In the first cycle the sharp peak is hydrogen adsorption peak at the 0.28 V and at the 0.40 V Tl dissolution. Peaks are suppressed faster during the potential cycling preferential Tl on step. After sixty cycles it suppressed and step can decorate. The hydrogen adsorption peak and the thallium peak height decreased and totally conclude.

The charge of (111) step sites for Tl/Pt crystal is ≈128 μC.cm^{-2} and for after preparation of Pt crystal is ≈176 μC.cm^{-2}. This is about 27% of the step-sites blocked by adsorbed Tl. The charge of (100) terrace sites for Tl/Pt crystal is ≈58 μC.cm^{-2} and

for after preparation of Pt crystal is ≈62μC.cm^{-2} .This is about %4 of the terrace-sites blocked by adsorbed Tl .The charge for the orientated defects sites for Tl/Pt crystal is ≈72 μC.cm^{-2} and for after preparation of Pt crystal is ≈99 μC.cm^{-2} .Tl is covered 27% from orientated defect sites. According to this result; Tl is blocked step-sites of Pt. There is no adsorption/desorption. At low concentration (1x10^{-6} M) difficult to say anything definite but that seems to be Tl preferentially adsorb at the step sites.

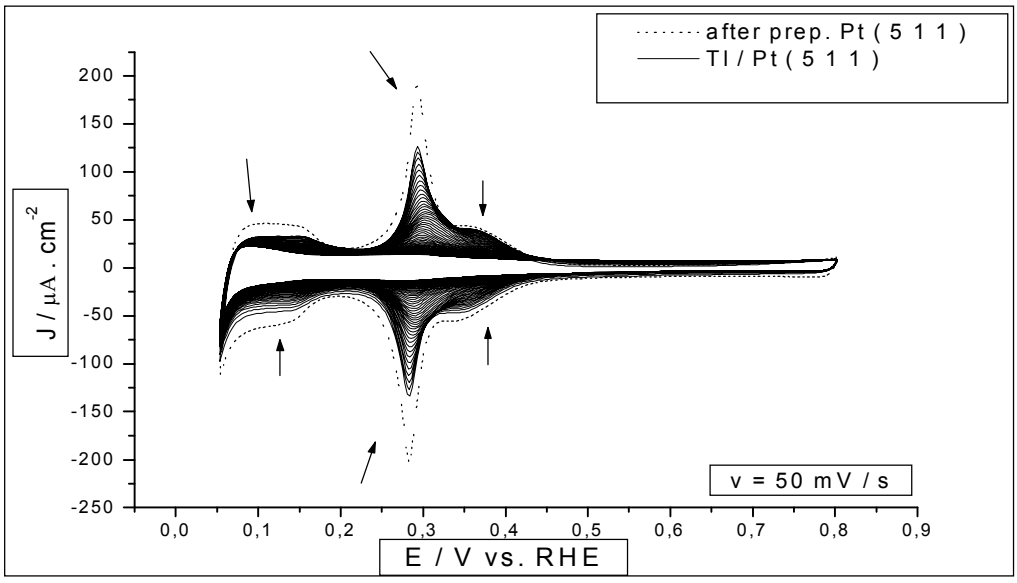


Figure 5.5. The CVs for Tl deposition (__) on Pt (511) in 1x10^{-6} M Tl_2SO_4 + 0.1 M H_2SO_4 and (. . .) after preparation in 0.1 M H_2SO_4 with v= 50 mV/s.

Figure 5.6. Shows the voltammogram of the underpotential deposition and desorption of Tl^+ in 1x10^{-6} M Tl_2SO_4 solution on a Pt (100) electrode at the potential range between 0.10 and 0.80 V. Due to the fact, that the adsorption time was too short, the blockage by Tl is incomplete in this very dilute solution. At the high potential maybe there is some peak but in this potential range there is not any peak.

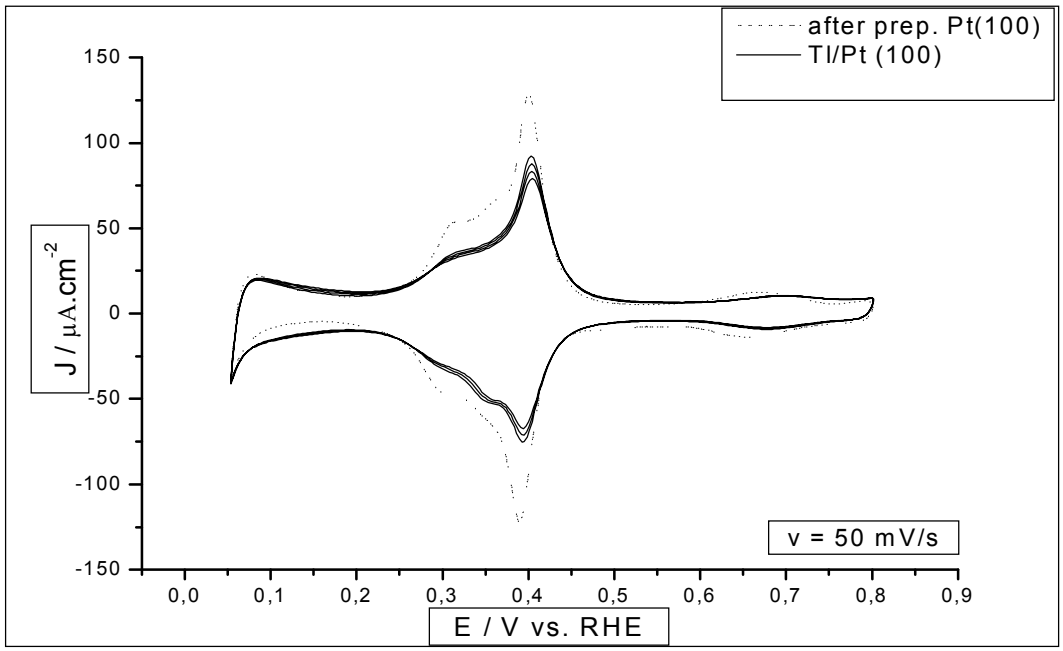


Figure 5.6. The CVs for Tl deposition (__) on Pt (100) in $1x10^{-6}$ M Tl_2SO_4 + 0.1 M H_2SO_4 and (. . .) after preparation in 0.1 M H_2SO_4 with v= 50 mV/s**.**

Figure 5.7. Shows the voltammogram of the underpotential deposition and desorption of Tl^+ in $1x10^{-3}$ M Tl_2SO_4 solution on a Pt (111) electrode at the potential range between 0.10 and 0.80 V with v=50 mV/s. In this figure can see directly, all peaks shifted more positive potential. Hydrogen is totally blocked.

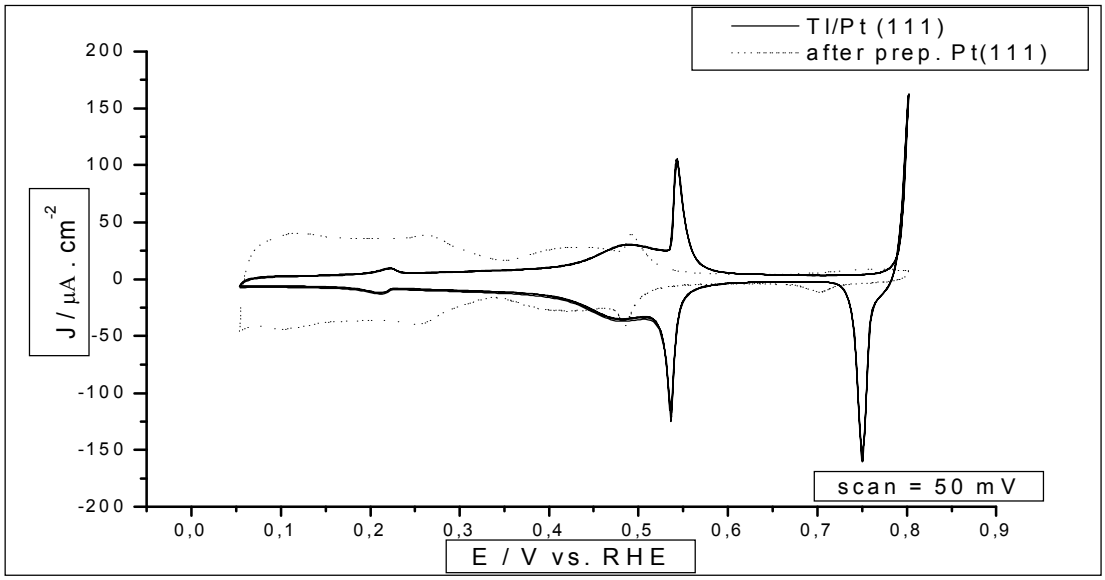


Figure 5.7. The CVs for Tl deposition (__) on Pt (111) in $1x10^{-3}$ M Tl_2SO_4 + 0.1 M H_2SO_4 and (. . .) after preparation in 0.1 M H_2SO_4 with v= 50 mV/s.

5.2. Pb UPD on Pt (100) and the stepped Pt single-crystal Pt (19,1,1), Pt (11,1,1) and Pt (511)

5.2.1. Voltammetry of the unmodified Pt bead single-crystals in perchloric acid

After preparation of the single-crystals by flame annealing, as described in chapter 5.1.1. , the different bead single- crystals are brought in contact with a 0.1 M $HClO_4$ at a potential of 0.05 V in a hanging meniscus configuration and CV is recorded with a sweep rate of 50 mV/s.

For the figure 5.8. Shows the voltammogram of the preparation for the Pt(S) [n(100)x(111)] with n = 3, 6 and 10 stepped single-crystal surfaces and Pt (100) surface. The CV are in good agreement with those previously reported by Clavilier and Domke et al [A. Rodes, (1991)] [K. Domke, (2003)]. The peak in the potential range between 0.25-0.5 V in the CV for the Pt (100) is related to hydrogen adsorption /desorption. The peaks in the potential range between 0.25 and 0.35 V

increase with increasing step-density, so do the peaks in the potential region between 0.05 and 0.25 V. These peaks are related to hydrogen adsorption/desorption on step-sites. The peaks between 0.35 and 0.50 V are related to hydrogen adsorption/desorption on the (100) terrace sites, and therefore decrease with increasing step density.

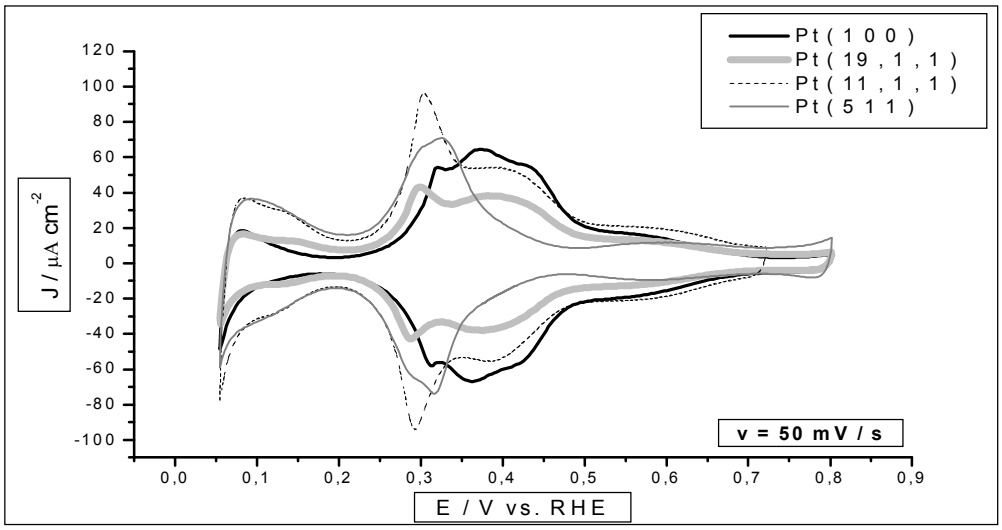


Figure 5.8. Voltammetric profiles of the Pt(S)[n(100) _ (111)] electrodes, with n = 3, 6, 10 and Pt (100) in 0.1 M $HClO_4$. Sweep rate = 50 mV/s.

Figure 5.9. In the potential range between 0.05 and 0.35 V vs. RHE hydrogen is adsorbed/desorbed .The small peaks at 0.10 and 0.32 V are related to hydrogen adsorption/ desorption on defect sites. At the 0.8 V in the CV is related to ClO_4^- adlayer. This CV is a good agreement with literature [R. Francke, (2008)].

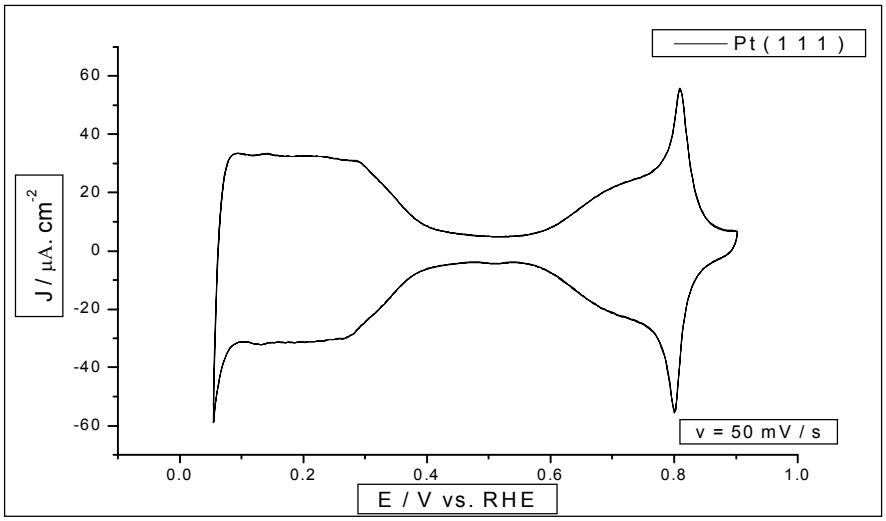


Figure 5.9. Recorded CVs Pt (111) in 0.1 M $HClO_4$ with v =50 mV/s.

For the CVs in figure 5.8. and 5.9. in the potential range between 0.10 and 0.50 V and for Pt (111) is between 0.10 and 0.70 V a charge-density of these CVs are integrated after correction of double-layer contribution and they are summarized in Table 5.2.

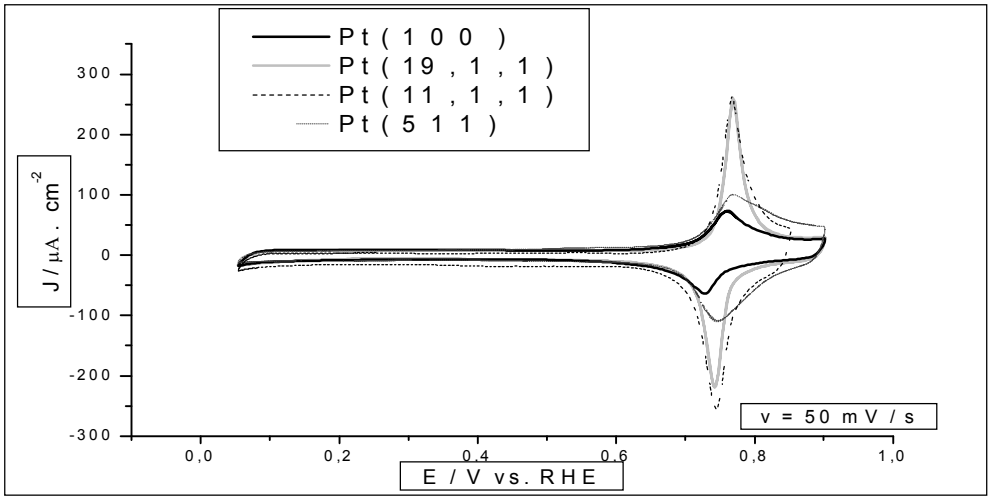
Table 5.2. Charge of various Pt-single crystals.

Single Crystal	**Charge / µC.cm^{-2}**
Pt (19,1,1)	≈198
Pt (11,1,1)	≈307
Pt (511)	≈242
Pt (100)	≈232
Pt (111)	≈221

5.2.2. Pb UPD on Pt(100), Pt(19,1,1), Pt(11,1,1) and Pt(511) from $Pb(ClO_4)_2$ contianing solution

Figure 5.10. a) and b) shows the voltammogram of the Pb-upd on the Pt(S)[n(100)x(111)] with n = 3 , 6 and 10 stepped single-crystal surfaces and Pt (100) surface with v = 10 mV/s and v = 50 mV/s recorded after immersion into a $1x10^{-3}$ M $Pb(ClO_4)_2$ containing 0.1 M $HClO_4$. In the potantial range between 0.5-0.85 V in the CV, no peaks for hydrogen are visible any more, instead a large peak at 0.76 V is visible, which is related to Pb adsorption and desorption. Pb totally blocks the surface for H-upd. At potentials above 0.80 V, the Pb dissolves as Pb^{2+}. With increasing step density on the Pt(S)[n(100)x(111)] surface, the sharp peak at around 0.76 V, assigned to Pb adsorption on the step sites, decreases. There is no further peak visible for the adsorption of Pb on the step-sites. This might be due to the fact that Pb is very large, as compared e.g. to copper, where for the underpotential deposition 2 peaks are visible -one for Cu UPD on the step sites and one for Cu UPD on the terrace sites, and is only adsorbed on the terrace sites. Another reason might be that Pb deposited on the step-sites desorbs at fairly higher potentials. The charge density for the Pb upd on the Pt (100) surface is much lower than the charge-density observed on the stepped surface. For the CV of the Pt (100); it seems to be a problem either in the preparation or with the electrolyte solution .If compare it to result of Markovic et al the peak should be much larger [N. M. Markovic, (1998)].

a)



b)

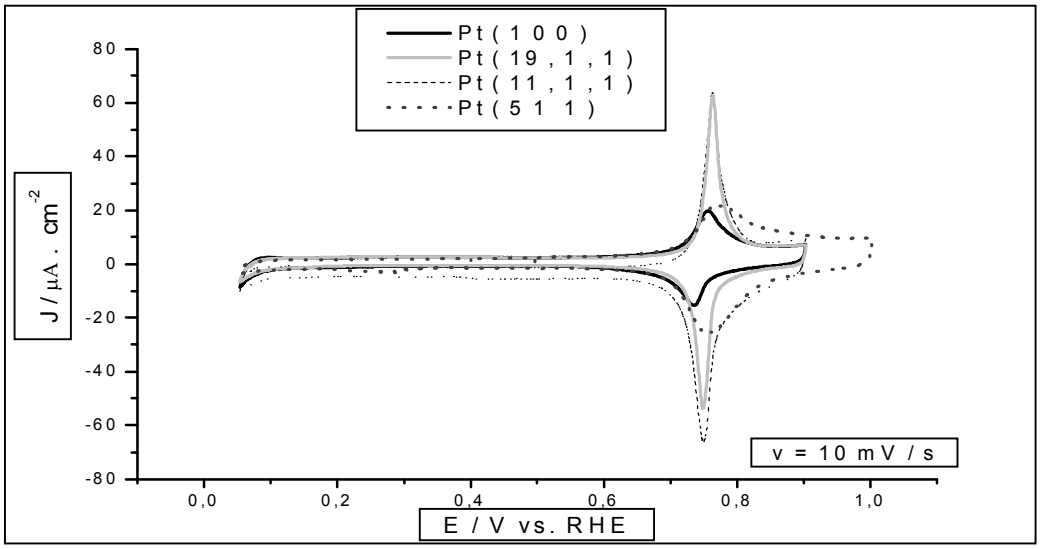


Figure 5.10. Voltammetric profiles of the Pt(S)[n(100)x(111)] electrodes, with n = 3, 6, 10 and Pt(100) in $1x10^{-3}$ M $Pb(ClO_4)_2$ + 0.1 M $HClO_4$ **a)** v = 50 mV/s. **b)** v = 10 mV/s.

Figure 5.11. a) and b) shows the voltammogram of the Pt (111) in $1x10^{-3}$ M $Pb(ClO_4)_2$ solution. At 0.65 V in the CV is related to Pb adsorption and desorption peaks. The total charge of anodic side is ≈301 $\mu C.cm^{-2}$**.** This is good agreement with

literature. Literature, where, a value of 304 μC.cm^{-2} is reported [B. N. Gurgur, (1997)] [H. Massong, (1998)].

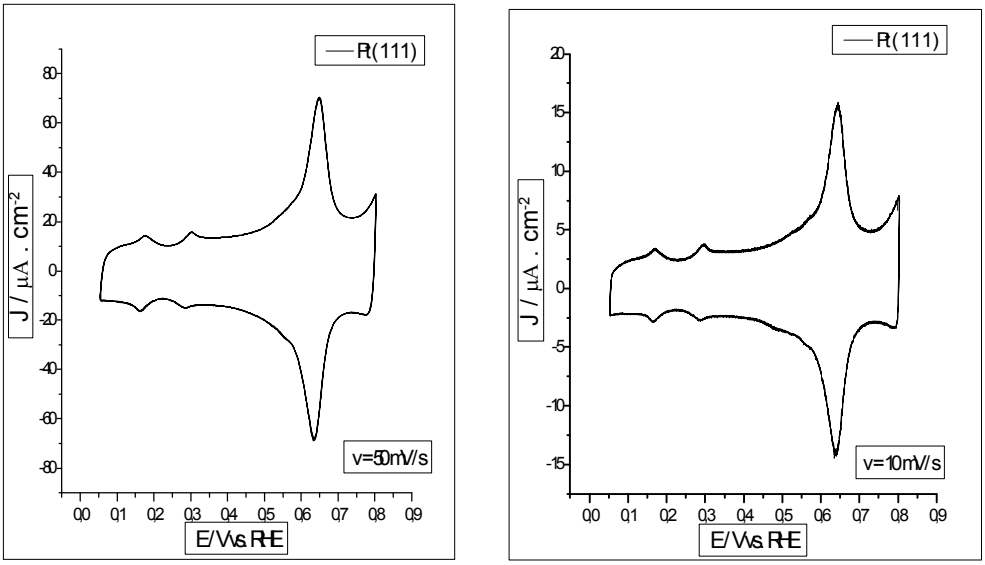


Figure 5.11. CVs for Pt (111) in 1x10^{-3} M $Pb(ClO_4)_2$ + 0.1 M $HClO_4$ with a) v= 50 mV/s b) v = 10 mV/s.

Table 5.3 shows the charge density of the UPD peaks comparison. In the potential range between 0.62 and 0.83 V and for Pt (111) is between 0.10 and 0.70 V a charge-density of these CVs are integrated after correction of double-layer contribuation and they are summarized in table 5.3. It should be noted there; due to correction of double-layer contribution, the charge value that is measured can be more or less than these value.

Table 5.3. Charge density of various Pt-single crystals

Single Crystals	**Charge / μC.cm^{-2} for V = 50 mV/s**	**Charge / μC.cm^{-2} for v = 10 mV/s**
Pt (19,1,1)	≈239	≈ 253
Pt (11,1,1)	≈ 261	≈ 258
Pt (511)	≈ 244	≈ 279
Pt (100)	≈ 159	≈177
Pt (111)	≈ 266	≈301

5.2.3. Cyclic Voltammetry of Pb / Pt-surfaces in $HClO_4$ solutions

Figure 5.12. shows the voltammogram of Pb/Pt in 0.1 M $HClO_4$ electrolyte the Pt(S) [n(100)x(111)] with n = 3 , 6 and 10 stepped single-crystal surfaces and Pt (100) after transferring the electrode back to the pure base electrolyte. It is immersed the electrodes form the Pb containing electrolyte at high potential. It is holded for a one or two minutes. It is rinsed the electrodes with MilliQ-water before immersion. Compared to the voltammograms of the clean Pt electrode, the hydrogen adsorption on step and terrace sites seem to be slightly blocked after performing the Pb upd experiments. This might be due to some residual Pb due to insufficient rinsing of the electrode before re-emmersion into to Pb free base electrolyte, or an incomplete desorption of Pb at the emmersion potential from the Pb containing electrolyte. Another possibility is, that due to the ongoing adsorption/desorption of Pb on the surface, the surface is roughened afterwards.

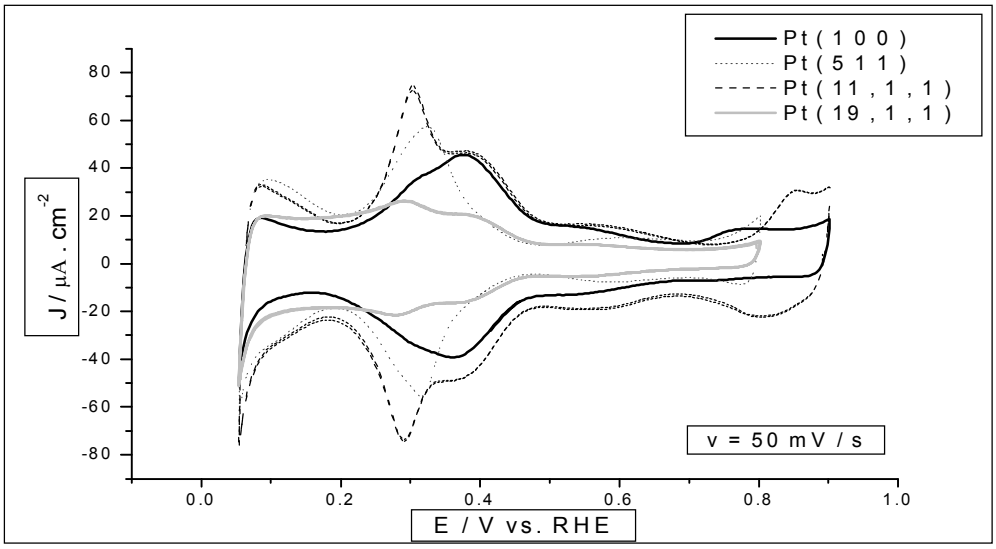


Figure 5.12. Voltammetric profiles of the Pt(S)[n(100)x(111)] electrodes, with n = 3, 6, 10 and Pt(100) after Pb-upd in 0.1 M $HClO_4$ with v = 50 mV/s.

The changes in the voltammogram is at it´s extreme for the Pt (111) surface, where the hydrogen and perchlorate adsorption/desorption are almost completely blocked after performing the Pb-upd experiments, as can be seen in figure 5.13.

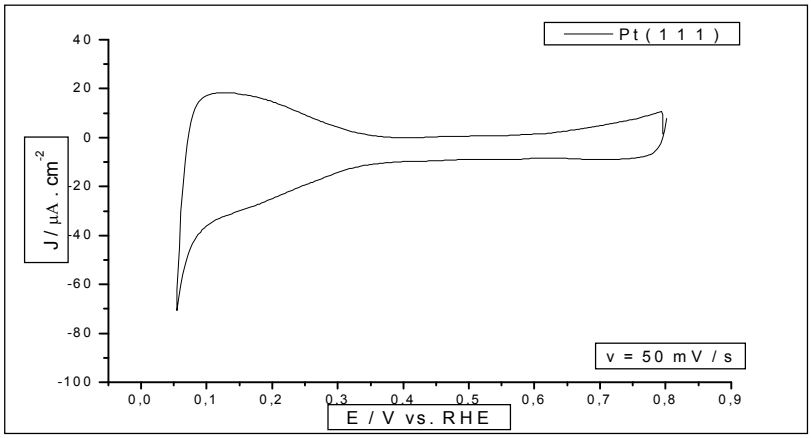


Figure 5.13. CVs for Pt (111) after Pb-upd in 0.1 M $HClO_4$ with v = 50 mV/s.

Table 5.4. Charge of various Pt-single crystals .The integration limit is between 0.10 and 0.50 V.

Single Crystals	**Charge / µC.cm^{-2}**
Pt (19 ,1 ,1)	≈153
Pt (11 ,1 ,1)	≈272
Pt (5 ,1 ,1)	≈220
Pt (1 ,0 ,0)	≈204

5.3. Effect of Ru submonolayers on the CO oxidation on Pt (19,1,1)

5.3.1. CO oxidation at the Ru free Pt(19,1,1) surfaces

Preparation process is the same step with Tl and Pb experiment. The single-crystal is heated in a flame and cool over a pure water in a hydrogen atmosphere. It is

good to giving bubble the electrolyte solution for a few seconds before forming a meniscus to remove any contaminants on the surface of the solution. We should make sure there is no water in the crystal holder or in the glass holder and we should never expose the glass holder to the flame during annealing the crystal to avoid forming contaminants that could be transferred to the electrolyte solution while making the meniscus contact.

Figure 5.14. Shows the voltammogram of the preparation for the Pt(S)[n(100)x(111)] with n = 10 stepped single-crystal surface in 0.1 M H_2SO_4 base-electrolyte with v = 50 mV/s. In the potential range between 0.05-0.35 V in the CV is related to hydrogen adsorption and desorption peaks at step sides. At 0.38 V in the CV is related to hydrogen adsorption/desorption peaks at terrace sites. Charge of the (111) terrace is ≈161 μC.cm^{-2}.In the CV in the potential between 0.10 and 0.55 V the all charge of anodic side is ≈352 μC.cm^{-2}.

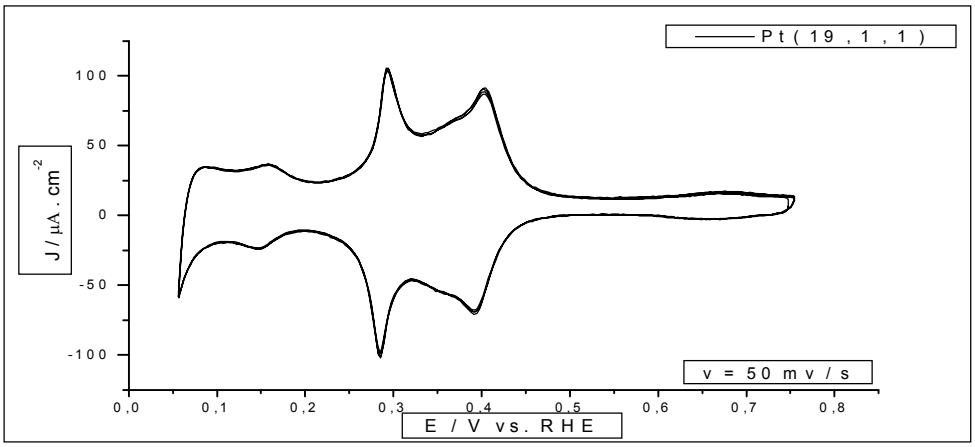


Figure 5.14. Recorded CVs for after preparation of Pt (19,1,1) in 0.1 M H_2SO_4 with v=50 mV/s.

After recording a CV in the sulphuric acid to check the preparation of the single-crystal, a CO oxidation experiments is performed on the Pt(19,1,1) surface. Therefore, holding the potential at 0.7 V, 2 mL of CO saturated 0.1 M H_2SO_4 where added to the H-cell. After adsorption of CO for 3 minutes the electrolyte in the cell is exchanged under potential-control, by opening the glass-cock at the bottom of the H-

cell, and at the same time adding new electrolyte to the cell via the electrolyte depot, maintaining the hanging-meniscus configuration. At least 3 times the cell-volume is exchanged. After CO adsorption, the potential-program is started again and a cyclic voltammogram for the CO oxidation is recorded. For the CO oxidation, a sharp peak at a potential of 0.75 V with a small shoulder at somewhat lower potential can be observed, having a charge-density of approximately 356μC.cm^{-2}. For the small shoulder between 0.64 and 0.72 V a charge 104 μC.cm^{-2} is integrated.

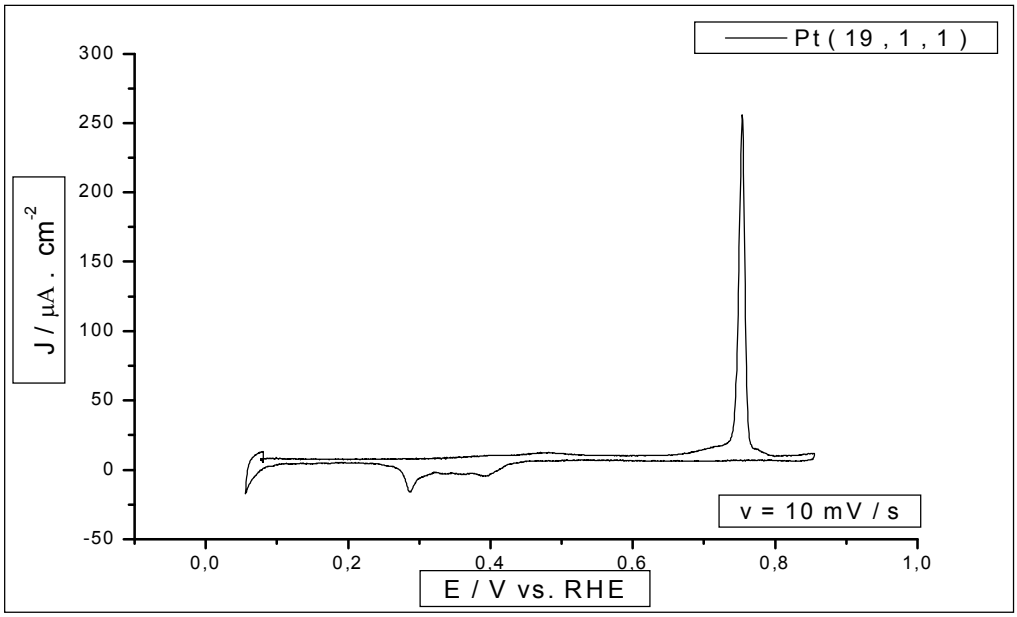


Figure 5.15. The first CV for Pt (19,1,1) after CO oxidation in 0.1 M H_2SO_4 with v= 10mV/s.

Figure 5.16. Shows the voltammogram after CO oxidation in 0.1 M H_2SO_4 with v = 50 mV/s. The charge in the potential between 0.15 and 0.50 V of the anodic is ≈317 μC.cm^{-2}. No altering of the surface due to the CO adsorption and oxidation can be observed.

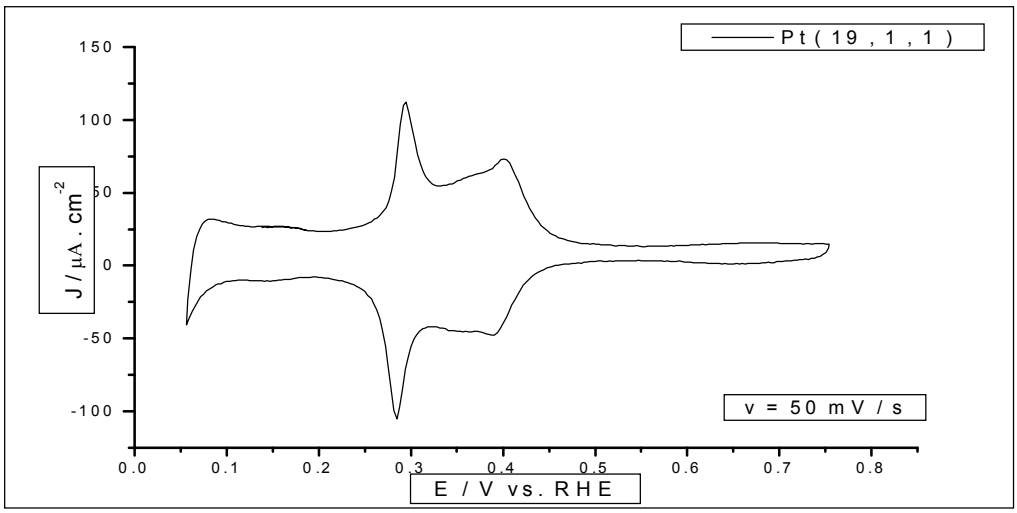


Figure 5.16. CVs for the Pt (19,1,1) for after CO oxidation in 0.1 M H_2SO_4 with v = 50 mV/s.

5.3.2. Adsorption of Ru submonolayers on Pt (19,1,1) surfaces

Figure 5.17. shows the CV for diffusion-controlled Ru-depositon on Pt (19,1,1) in a $1x10^{-5}$ M $RuCl_3$ in 0.1 M H_2SO_4 during potential-cycling in the potential range of 0.05 to 0.80 V after emersion of the electrode at 0.80 V. Already in the first cathodic sweep, a large peak at a potential of 0.30 V and a small peak at a potential of 0.24 V is visible. The corresponding peaks can be obtained in the anodic sweep; althought the peak at 0.35 V is not as sharp as in the cathodic sweep. The difference between cathodic and anodic scan might be related to chloride adsorption on the surface. With ongoing Ru-deposition the current-density in the potential range between 0.05 and 0.15 V, related to hydrogen adsorption/desorption on the Pt(19,1,1) surface, is more and more suppressed, and also the charge density for both peaks. The whole cyclic voltammogram is shifting up, because during transfer traces of oxygen, which lead to a negative charge due to reduction of this oxygen, are reduced. The cathodic sweep is not effected that much by this extra-process. New peak features for the deposited Ru appear at 0.58 and 0.64 V, related to OH-adsorption on the Ru [G. Samjeske, (2002)] [J. S. Spendelow, (2004)]. Ru is

deposited as Ru 3D island with a usual diameter of 2 mm diameter. In the CV between 0.10 and 0.45 V charge density in the anodic side is ≈202 μC.cm^{-2}.

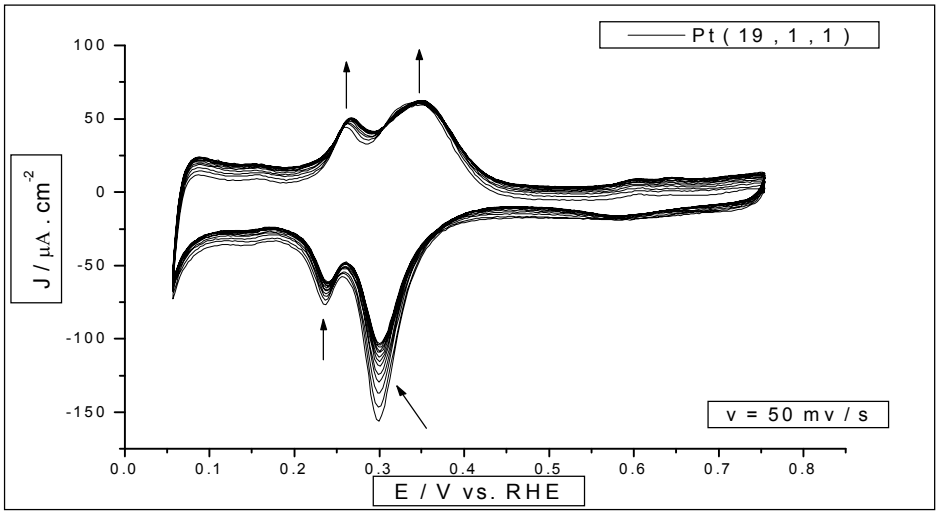


Figure 5.17. CVs for Ru-deposition at Pt (19,1,1) in 1x10^{-5} M $RuCl_3$ + 0.1 M H_2SO_4 with v= 50 mV/s.

5.3.3 Voltammogram of the Ru/Pt (19,1,1) electrode in H_2SO_4

After Ru-deposition, a CV is recorded in ruthenium-free base-electrolyte. Figure 5.18. compares the CV before and after Ru-deposition. The adsorption of Ru seems to block the surface for H up. In the potential range between 0.10 and 0.50 V, after the Ru deposition a charge of ≈172 μC.cm^{-2} is integrated, in the same potential range after preparation a charge of 360 μC.cm^{-2} can be integrated. Two new peaks are for the Ru adsorbate are visible at 0.60 and 0.70 V.

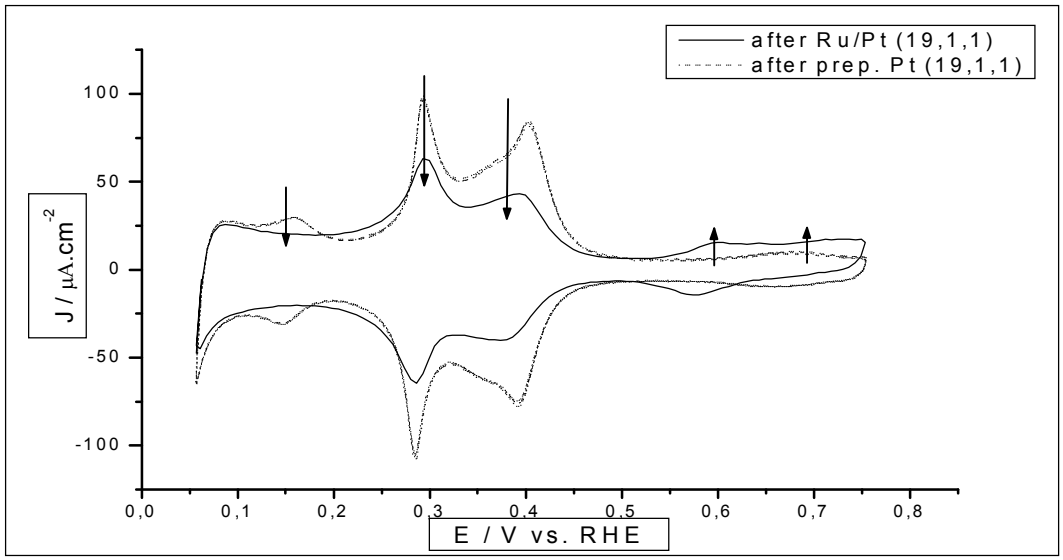


Figure 5.18. The CVs for Ru / Pt (19,1,1) in 0.1 M H_2SO_4

CO oxidation

After the deposition of Ru on the Pt (19,1,1)-surface, CO oxidation experiments are performed on the Ru/Pt (19,1,1) surface. Therefore, holding the potential at 0.07 V, 2 mL of CO saturated 0.1 M H_2SO_4 where added to the H-cell. After adsorption of CO for 3 minutes the electrolyte in the cell is exchanged under potential-control, by opening the glass-cock at the bottom of the H-cell, and at the same time adding new electrolyte to the cell via the electrolyte depot, maintaining the hanging-meniscus configuration. At least 3 times the cell-volume is exchanged. After CO adsorption, the potential-program is started again and a cyclic voltammogram for the CO-oxidation is recorded. Figure 5.19. shows the voltammogram, where two peak for the CO-oxidation can be observed, the first one with a small shoulder at lower potential.

In the CV at the potential 0.55 and 0.63 V charge of the sharp peak is ≈215 $\mu C.cm^{-2}$ for Pt(19,1,1) . In the CV at the potential 0.63 and 0.73 V charge of peak is ≈170 $\mu C.cm^{-2}$ and between 0.50 and 0.58 V charge of peak is 77 $\mu C.cm^{-2}$. In the potential range between 0.50 and 0.73 V the whole anodic charge is ≈462 $\mu C.cm^{-2}$.

In the second anodic sweep no more peaks for CO oxidation are visible, indicating that the electrolyte exchange was successful, and there is no residual CO in solution.

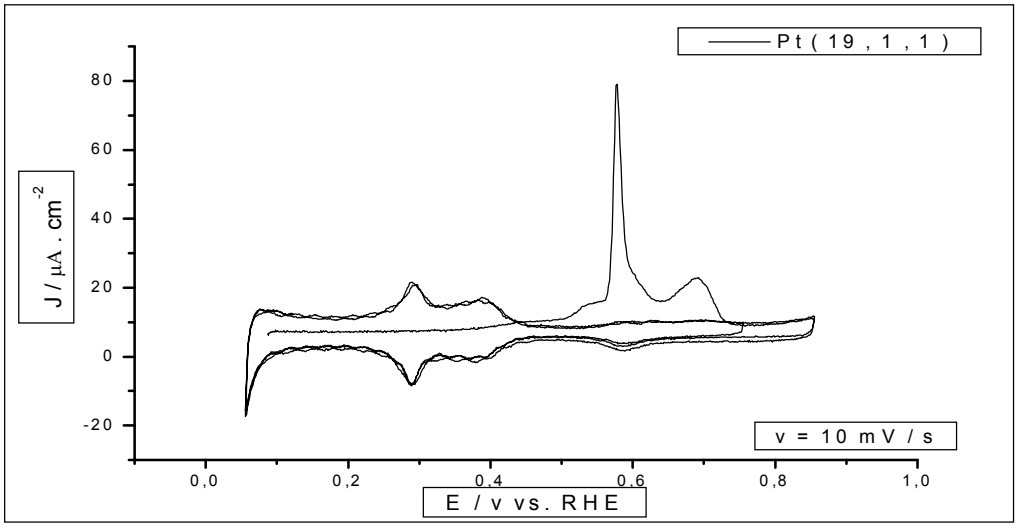


Figure 5.19. The CVs for CO oxidation in 0.1 M H_2SO_4 with v= 10 mV/s.

A second experiment on the CO oxidation is performed, where after adsorption of the CO at 0.07 V and starting the potential-program, the potential-program is stopped again in the beginning of the first CO oxidation peak at 0.54 V for 3 minutes before starting the potential-program again. The result of this experiment is shown in figure 5.20**.** It can be easily distinguish to Ru effect with this cyclic voltammogram.

Performing the second potential stop, the second peak for CO oxidation at around 0.70 V seems not to be affected. This indicates that there are two different adsorption vicinities for CO on the surface, which can be oxidized separately.

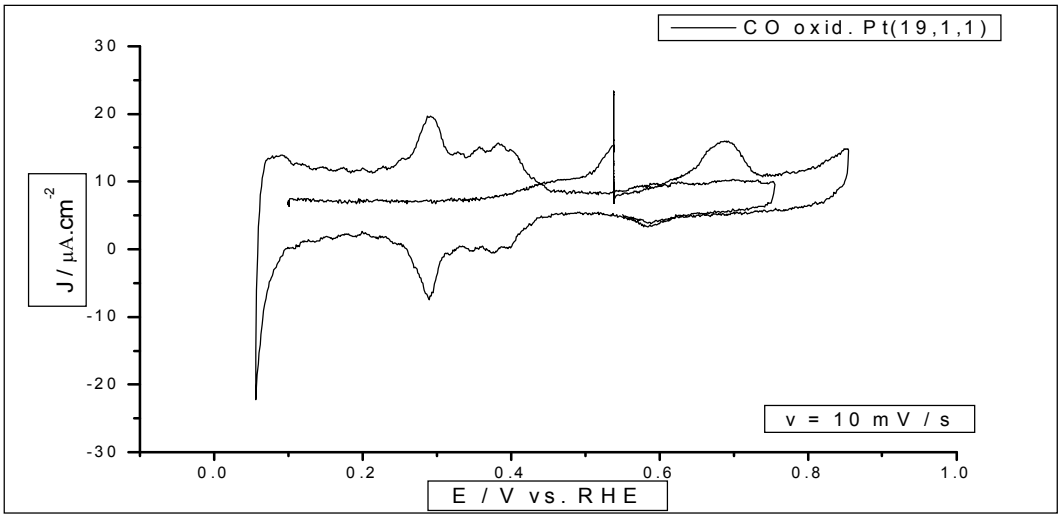


Figure 5.20. The CV for CO oxidation of Pt (19,1,1) with v=10mV/s.

Figure 5.21**.** Shows after CO oxidation, we found no indication for a change of the Ru modified surface, as compared to the CV record before CO oxidation.

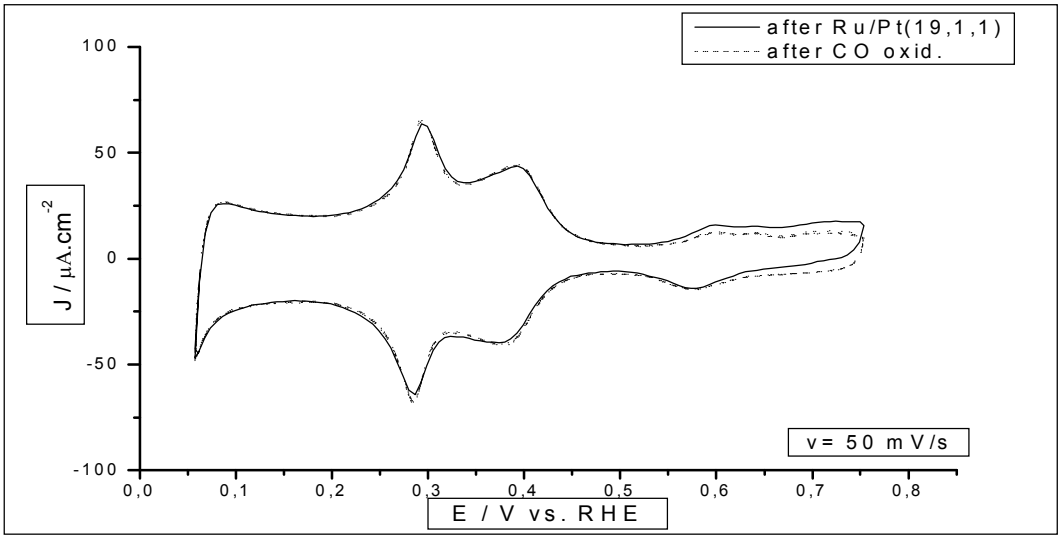


Figure 5.21. The CV for the Pt (19,1,1) (. . .)after CO oxidation and (__) after Ru/Pt in 0.1 M H_2SO_4 with v = 50 mV/s

5.4. Discussion

Effect of Ru on the CO oxidation at Pt (19,1,1)

As compared to the CO oxidation at the Ru-free surface, CO oxidations starts at much lower potentials, approximately 0.25 V lower in potential. This is best resembled in figure 5.22.

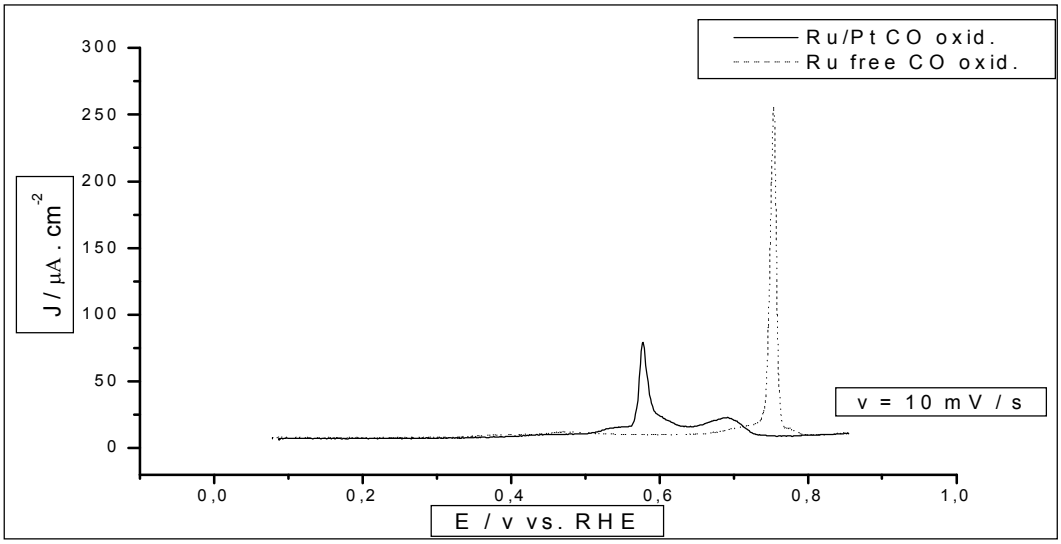


Figure 5.22. Compares the CO oxidation (….) Ru free surface and (___) Ru containing solution with v=10 mV/s.

Similar results for the CO oxidation, holding the potential at the beginning of CO oxidation, at Ru modified Pt(S)[(111)x(111)] where reported by Massong on Lanova et al [H. Massong, (2000)] , [B. Lanova and H. Baltruschat, (2008)]. They related this effect to two different adsorption sites for the CO adsorbate: one in the vicinity of Ru, and one far away from Ru. The catalytic effect of Ru is explained by the so called bifunctional mechanism. On the one hand, Ru has an electronic effect, and modifies the binding energy of the adsorbed CO. On the other hand, oxygen-species adsorbed on Ru, can easiliy promote CO oxidation to CO_2 on the Pt sites by a spillover of this oxygen-species. Therefore the CO next to Ru is oxidized at much

lower potential than CO adsorbed far away from Ru. This is observed here for the first time for CO oxidation on a stepped Pt(S)[n(100)x(111)] surface, the Pt(19,1,1).

For Pb experiments terrace decoration is possible with Pb. For Pb-UPD with increasing step density Pb adsorption decreases. At potentials above 0.80 V, the Pb dissolves as Pb^{2+}.If after preparation is compared with after Pb/Pt, that the original shape of the hydrogen peaks are shifted and surfaces blocked by Pt. For Pt(111) ; it seems to be a problem. It can due to maybe it is immersed at low potential.

For Tl experiments step decoration is possible with Tl. Tl preferential decorate on step-sites. For Tl/Pt (111); all peaks shifted more positive potential and hydrogen totally blocked.

6. SUMMARY

In the past only Pt(111), Pt(100) was investigated, but in the present thesis , the effect of step sites on the Tl and Pb upd on stepped Pt surfaces vicinal to the (100) surface are studied. A comparison of these metals has been made. Tl decorated on step-sites but for Pb it can be commented that it preferential orientated to decorate on terrace-sites. For Pb-upd (100) surface is higher than (111) surface. It can be due to adsorption geometry difference. Pb adsorption is more stable at (100) surface than (111) surface. Because there is a big desorption potential difference.

CO oxidation experiments are performed on the Ru/Pt (19,1,1) surface. For the CO oxidation on Pt (19,1,1), the catalytic effect of Ru is investigated. Onset of the CO oxidation, two peaks instead of one, first peak can be oxidized separately; by bifunctional mechanism Ru accelerates the CO oxidation on step sites by decreasing the activation energy. Second peak is not affected by Ru. Electronic effect of Ru is, it destabilize the CO molecules adsorbed on the vicinity of Ru. It is observed new peaks due to Ru adsorption.

From the experiment I performed some questions, which could not be answered completely. For the stepped single-crystal are the peaks really related to adsorption on terraces/steps? How perfect are these metals-upd CVs? For Pb-upd why it can not be observed H-upd on step-sites?

REFERENCE

BITTNER A. M. , WINTTERLIN J. , and ERTL G. , (1997) Surface Science, 376:267.

BLAKELY D. W. and SOMORJAİ G. A. , (1977), Surface Science 65:419.

BOGOLOWSKI N. , HUXTER S. , ATTARD G. , and BALTRUSCHAT H., (2008).

CASADESUS M. , (2009), Journal of Electroanalytical Chemistry 625:123.

CLAVILIER J. , (1980), Journal of Electroanalytical Chemistry 107:211.

CLAVILIER J. and ARMAND D. , (1986), J ELECTROANAL CHEM 199:187.

CLAVILIER J. , FAURE R. , GUINET G. , and DURAND R. , (1980), Journal of Electroanalytical Chemistry 107:205.

CLAVILIER J. , GANON J.-P. , and PETIT M. , (1989), Journal of Electroanalytical Chemistry 265:231.

DOMKE K. , HERRERO E. , RODES A., and FELIU J. M. , (2003), Journal of Electroanalytical Chemistry 552:115.

FELIU J. M. , ORTS J. M. , GOMEZ R. , ALDAZ A. , and CLAVILIER J. , (1994), Journal of Electroanalytical Chemistry 372:265.

FIORENTINI V. , METHFESSEL M. , and SCHEFFLER M. , (1993), Physical Review Letters 71:1051.

FRANCKE R. , CLIMENT V. , BALTRUSCHAT H. , and FELIU J. M. , (2008), Journal of Electroanalytical Chemistry and Interfacial Electrochemistry 624:228.

FUNTIKOV A. M. , LINKE U. , STIMMING U. , and VOGEL R. , (1995) , Surface Science 324:L343.

FUNTIKOV A. M. , STIMMING U., and VOGEL R. , (1997), Journal of Electroanalytical Chemistry 428:147.

FURUYA N. and KOIDE S. , (1989), Surface Science 220:18.

GASTEIGER H. A. , MARKOVIC N. , ROSS P. N. , and CAIRNS E. J. , (1993), Journal of Physical Chemistry 97:12020.

GURGUR B. N. , MARKOVIC N. M. , and ROSS P. N. , (1997) , Langmuir

13:6370.

HAZZAZI O. A. , ATTARD G. A. , WELLS P. B. , VIDAL-IGLESIAS F. J. , and ROSS P. N. and WAGNER F. T. , in Advances in Electrochemistry and Electrochemical Engineering. XIII, Vol. XIII (H. Gerischer and C. W. Tobias, eds.), Wiley-Interscience, N. York, 1984, p. 70.

HERNANDEZ F. and BALTRUSCHAT H. , (2006) Langmuir 22:4877.

JENKINS S. J. , PETERSEN M. A. , and KING D. A. , (2001), Surface Science 494:159.

KIBLER L. A. , (2003), Preparation and Characterization of Noble Metals Single Crystal Electrodes, University of Ulm.

LANOVA B. , (2009) , in Institute für Physikalische und Theoretische Chemie, Abteilung Elektrochemie, Vol. Ph.D., Rheinische Friedrich-Wilhelms Universität Bonn, Germany.

LANOVA B. and BALTRUSCHAT H. , (2008).

MARKOVIC N. M. , GURGUR B. N. , LUCAS C. A. , and ROSS P. N. , (1998), Journal of the Chemical Society-Faraday Transactions 94:3373.

MASSONG H. , TILLMANN S. , LANGKAU T. , MEGUID E. A. Abd El, and BALTRUSCHAT H. , (1998) Electrochimica Acta 44:1379.

MASSONG H. , WANG H. S. , SAMJESKE G. , and BALTRUSCHAT H. , (2000) Electrochimica Acta 46:701.

MICHAELIS R. and KOLB D. M. , (1992), Journal of Electroanalytical Chemistry 328:341.

MICHAELIS R. , ZEI M. S. , ZHAI R. S. , and KOLB D. M., (1992), Journal of Electroanalytical Chemistry 339:299.

MICHELY T. and COMSA G. , (1991), Surf. Sci. 256:217.

ODA I. , SHINGAYA Y. , MATSUMOTO H. , and ITO M. , (1996), J.Electroanal. Chem. 409:95.

PRATT S. J. , JENKINS S. J. , and KING D. A. , (2005), Surface Science 585:L159.

RODES A. , ZAMAKHCHARI M. A. , ACHI K. El , and CLAVILIER J. , (1991), Journal of Electroanalytical Chemistry 305:115.

SAMJESKE G. , XIAO X.-Y. , and BALTRUSCHAT H. , (2002), Langmuir

18:4659.

SASHIKATA K. , FURUYA N. , and ITAYA K. , (1991), Journal of Electroanalytical Chemistry 316:361.

SASHIKATA K. , FURUYA N. , and ITAYA K. , (1991), J. Vac. Sci. Technol. B 9:457

SOMORJAİ G. A. , (1994), Surface Science 299/300:849.

SOMORJAİ G. and BLAKELY D. W. , (1977), Surface Science 65:419.

SORIAGA M. P. , (1992), Surface Science 39:325.

SPEK A. L. , (2003), Journal of Applied Crystallography , 36:7

SPENDELOW J. S. and WIECKOWSKI A. , (2004), Physical Chemistry Chemical Physics 6:5094.

SWAMY K. , BERTEL E., and VILFAN I., (1999), Surface Science 425:L369.

TIAN N. , ZHOU Z.-Y. , and SUN S.-G. , (2008), The Journal of Physical Chemistry C 112:19801.

WARD L. C. and STICKNEY J. L. , (2001), Physical Chemistry Chemical Physics 3:3364.

WHEELER D. R. , WANG J. X. , and ADZİC R. R. , (1995) Journal of Electroanalytical Chemistry 387:115.

YAU S. L. , KIM Y. G. , and ITAYA K. , (1996), Journal of the American Chemical Society 118:7795.

http://www.mateck.de

http://www.lenntech.com/Periodic-chart-elements/pb-en.htm

CURRICULUM VITAE

İpek KILIÇCI was born in Adana in 1985. She finished primary school in 'DSİ Primary school' and She continued intermediate and high school in 'Seyhan Rotary Anatolian High School'. She graduated at 2003 and this year she started chemistry in University of Çukurova a Master Degree at 2003. After she finished BSc, she started to master degree of chemistry in Institute of Naturel and Applied Sciences University of Çukurova in 2007. At 2008 she studied in Bonn University for second year of my master via erasmus program.